

# RefAtomNet++: Advancing Referring Atomic Video Action Recognition using Semantic Retrieval based Multi-Trajectory Mamba

Kunyu Peng Di Wen Jia Fu Jiamin Wu Kailun Yang Junwei Zheng Ruiping Liu  
Yufan Chen Yuqian Fu Danda Pani Paudel Luc Van Gool Rainer Stiefelhagen

**Abstract**—Referring Atomic Video Action Recognition (RAVAR) aims to recognize fine-grained, atomic-level actions of a specific person of interest conditioned on natural language descriptions. Distinct from conventional action recognition and detection tasks, RAVAR emphasizes precise language-guided action understanding, which is particularly critical for interactive human action analysis in complex multi-person scenarios. In this work, we extend our previously introduced RefAVA dataset to RefAVA++, which comprises  $> 2.9$  million frames and  $> 75.1k$  annotated persons in total. We benchmark this dataset using baselines from multiple related domains, including atomic action localization, video question answering, and text-video retrieval, as well as our earlier model, RefAtomNet. Although RefAtomNet surpasses other baselines by incorporating agent attention to highlight salient features, its ability to align and retrieve cross-modal information remains limited, leading to suboptimal performance in localizing the target person and predicting fine-grained actions. To overcome the aforementioned limitations, we introduce RefAtomNet++, a novel framework that advances cross-modal token aggregation through a multi-hierarchical semantic-aligned cross-attention mechanism combined with multi-trajectory Mamba modeling at the partial-keyword, scene-attribute, and holistic-sentence levels. In particular, scanning trajectories are constructed by dynamically selecting the nearest visual spatial tokens at each timestep for both partial-keyword and scene-attribute levels. Moreover, we design a multi-hierarchical semantic-aligned cross-attention strategy, enabling more effective aggregation of spatial and temporal tokens across different semantic hierarchies. Experiments show that RefAtomNet++ establishes new state-of-the-art results, achieving 43.71%/42.52% (mIoU), 56.83%/59.81% (mAP), and 71.27%/75.72% (AUROC) on the validation/test sets of RefAVA, and 39.12%/38.58%, 58.24%/58.84%, and 72.58%/73.28% on the validation/test sets of RefAVA++, respectively, while maintaining high computational efficiency over prior state-of-the-art models. The dataset and code are released at [refAVA++](https://refava++.github.io).

**Index Terms**—Vision Language Model, Action Recognition, Video Understanding, State Space Model.

## 1 INTRODUCTION

Referring scene understanding [1], [2], [3], [4] aims to ground natural language *referring expressions* to specific elements in a visual scene, enabling models to reason selectively about objects or regions mentioned in text. Such capability is fundamental for bridging human-computer interaction, as context-driven queries provide an intuitive and efficient way for users to communicate with intelligent systems. This is particularly valuable for applications in information retrieval, assistive technologies, and multimedia analysis, where accurate alignment between textual queries and visual content is critical. Despite this potential, incorporating referring expressions into computer vision models poses significant challenges due to the complex entanglement among linguistic semantics, spatial localization, and visual recognition. The difficulty is further exacerbated in dynamic and cluttered

environments, where ambiguity in descriptions and inter-object dependencies requires more sophisticated grounding mechanisms.

Over the past years, several benchmarks have been developed to advance referring scene understanding across different domains. For example, benchmarks have been proposed for multi-object tracking with natural language queries [5], semantic segmentation with referring expressions [6], [7], [8], [9], [10], medical imaging scenarios requiring reference-based diagnosis [11], and object detection guided by textual instructions [12], [13], [14]. While these benchmarks have demonstrated substantial progress, they remain largely object-centric, focusing on static object localization or delineation given a descriptive phrase. However, many practical applications demand a shift from object-level reasoning toward human-centric understanding, where the task involves not only recognizing who is being referred to but also interpreting their fine-grained actions. This is especially critical in domains such as rehabilitation assistance [15], [16], where accurate understanding of patient actions is key to monitoring and guidance, and in human-robot interaction [17], [18], where robots must dynamically interpret human instructions and actions to achieve seamless collaboration.

The field of human action recognition has witnessed rapid progress, driven both by the emergence of powerful transformer-based architectures [19], [20], [21], [22], [23], [24], [25] and by the release of large-scale benchmark datasets [26], [27], [28], [29], [30]. For the study of atomic actions, datasets often contain

- *K. Peng, D. Wen, J. Zheng, R. Liu, Y. Chen, and R. Stiefelhagen are with the Institute for Anthropomatics and Robotics, Karlsruhe Institute of Technology, Germany.*
- *J. Fu is with the RISE Research Institutes of Sweden and the KTH Royal Institute of Technology, Sweden.*
- *K. Yang is with the School of Artificial Intelligence and Robotics and also with the National Engineering Research Center of Robot Visual Perception and Control Technology, Hunan University, China.*
- *J. Wu is with the Chinese University of Hong Kong, Hong Kong, and also with Shanghai AI Lab, China.*
- *K. Peng, Y. Fu, D. P. Paudel, and L. Van Gool are with INSAIT, Sofia University “St. Kliment Ohridski”, Bulgaria.*
- *Corresponding authors: Kunyu Peng and Kailun Yang.*

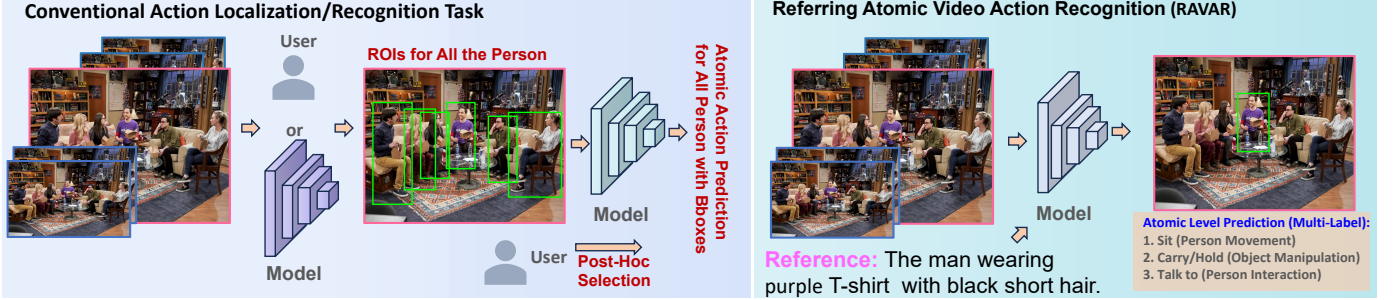


Fig. 1: Comparison between the AAL task (left) and the RAVAR task (right) reveals a key difference in approach. Traditional atomic action recognition in multi-person settings is usually framed as an action localization problem: regions of interest for each individual must first be identified, followed by per-person action classification and post-processing to isolate the target subjects. In contrast, RAVAR accepts a textual reference together with a video as input and jointly outputs both the atomic actions and the spatial location of the referred individual. This design underscores RAVAR’s efficiency by leveraging textual guidance; it eliminates much of the manual effort required for subject identification and enables focused analysis of the atomic actions for the individual of interest.

videos featuring multiple individuals engaged in simultaneous activities [31]. Despite this, the majority of existing approaches [19], [20], [25], [32], [33] either depend on manually cropped video windows for the person of interest or utilize automatically generated Regions Of Interest (ROIs) to predict atomic actions for all persons in a scene. These approaches require either significant preprocessing to isolate the individual of interest or redundant computation across all individuals, followed by postprocessing to extract results for the desired person, thereby introducing substantial inefficiency.

In this context, the Atomic Action Localization (AAL) task is typically constrained by the need for either user-provided guidance or automatically detected ROIs, both of which still rely on human postprocessing to identify the target individual after predictions are obtained. This workflow also poses significant limitations in certain real-world applications, such as assistive technologies for individuals with visual impairments [34], [35], [36], where it is essential to understand the state and actions of specific persons in the scene to enable effective interaction. A promising alternative lies in leveraging concise natural language descriptions that incorporate broad positional cues (*e.g.*, left, center, right), appearance-based attributes (*e.g.*, hair color, clothing), or demographic indicators (*e.g.*, gender) to directly guide the model toward the intended target. By using such textual references, the model can perform end-to-end retrieval of the specified individual throughout the video and subsequently deliver accurate atomic action recognition results, thereby eliminating redundant computation and reducing the need for human intervention.

To address this gap, our prior work introduced the task of **Referring Atomic Video Action Recognition (RAVAR)**, with key differences from conventional atomic action localization illustrated in Fig. 1. Unlike other prior work benchmarks that primarily focus on grounding objects [37], our formulation explicitly utilizes natural language queries as reference to the desired person, requiring models to not only localize the referred person but also disambiguate and classify their atomic actions. This problem setting introduces additional challenges, as the model must jointly resolve cross-modal alignment of language reference information and video information in multi-person and cluttered environments. As mentioned earlier, traditional approaches in multi-person settings typically operate within a localization framework, requiring predefined ROIs for each

individual before performing action recognition, followed by post-processing to isolate the person of interest. In contrast, RAVAR takes a video and a textual reference as inputs and directly outputs both the atomic actions and the location of the specified individual, thus improving efficiency by reducing labor-intensive subject identification. To benchmark this task, we established RefAVA in our previous work [38], built from 17,946 video clips of the AVA dataset [31], extended with 36,630 textual descriptions as referring expressions. The dataset spans diverse contexts, *e.g.*, indoor/outdoor and day/night scenarios, as well as rich multi-person interactions, making it a comprehensive testbed for the referring atomic video action recognition task. In our prior work [38], we also established the first RAVAR benchmark by evaluating 15 approaches from related domains and showed that none achieved satisfactory performance due to difficulties in suppressing irrelevant visual information. To overcome this, we proposed RefAtomNet [38], a model that jointly leverages textual referring expressions, visual features, and novel location-semantic tokens, while introducing cross-stream agent attention and token fusion to effectively align and filter multimodal information. However, the scope of data of our previous work is limited, and the proposed approach still suffers from its semantic visual retrieval capability to pursue more precise localization and fine-grained action prediction for the referred person.

To further advance the research in this area, in this work, we extend our previously introduced RefAVA dataset [38] into the enhanced RefAVA++ dataset by doubling the total number of annotated persons. Using this extended dataset, we systematically re-evaluated all previously adopted baselines as well as our earlier model, RefAtomNet [38]. Experimental results indicate that RefAtomNet [38] continues to outperform alternative baselines on RefAVA++. However, its semantic-visual-retrieval capability remains suboptimal. Specifically, while cross-modal agent attention highlights important tokens, it struggles to achieve precise alignment between textual-reference details and visual evidence, thereby limiting the model’s ability to robustly and efficiently localize the referred individual and to perform fine-grained atomic action reasoning. This highlights the need for a more advanced method to enhance semantic-retrieval and cross-modal alignment in RAVAR.

To tackle this problem, we propose RefAtomNet++, a framework built upon the vision-language model BLIPv2 [39]. The

model introduces a multi-trajectory semantic-retrieval Mamba to aggregate visual and linguistic tokens, and integrates a multi-hierarchical semantic-aligned cross-attention module to enable spatio-temporal reasoning across multiple semantic hierarchies in a more fine-grained manner. In particular, we consider three hierarchies of semantics: the holistic-sentence level, the partial-keyword level, and the scene-attribute level. For the holistic-sentence level, semantic tokens are derived by encoding the complete sentence with the BLIPv2 textual encoder [39]. The partial-keyword-semantic tokens are derived by first processing the reference sentence to remove stop words that do not contribute meaningful semantics, such as articles and prepositions. The remaining keywords, which usually correspond to salient entities or actions, are then passed through an LLM-based textual encoder to obtain fine-grained keyword-level embeddings. These embeddings serve as partial semantic tokens, providing more localized guidance than the holistic-sentence representation. For the scene-attribute level, we utilize a pretrained object detector, *i.e.*, DETR [40], to identify objects present in the key frame, which is selected as the temporal center of the video to capture representative contextual information. For each detected object, we combine the spatial information encoded by its bounding box coordinates with its categorical embedding obtained from the textual encoder along channel dimension. This fusion yields the scene-attribute-semantic tokens, which explicitly encode object-centric context and their spatial arrangement, thereby complementing both the holistic-sentence and partial-keyword representations.

To prune irrelevant visual tokens for a more concrete feature aggregation upon different semantic hierarchies, we use both the partial-keyword-semantic tokens and the scene-attribute-semantic tokens to retrieve the relevant spatial-temporal visual tokens obtained from the vision-language models, and we select the most similar visual token from the spatial dimension for each keyword/attribute token and each time step to formulate semantic-aligned-visual trajectories. Then, we adopt Mamba [41] to achieve the multi-trajectories feature aggregation, as Mamba [41]. State-space modeling used in Mamba provides a continuous and memory-efficient mechanism to aggregate multiple semantic trajectories by capturing long-range temporal dependencies with stable dynamic transitions, which are essential for fine-grained action reasoning in videos. Unlike discrete attention mechanisms, the state-space formulation enables smooth temporal filtering and coherent aggregation of different trajectories, aligning them into a unified latent representation that preserves the temporal continuity of fine-grained human actions. After that, we obtain the scene-attribute-retrieved visual tokens and the partial-keyword-retrieved visual tokens following the same manner.

To effectively exploit contextual visual cues, we further propose a multi-hierarchical semantic-aligned cross-attention mechanism. Specifically, the holistic-sentence-semantic visual tokens, the scene-attribute-semantic visual tokens, and the partial-keyword-semantic visual tokens are employed as queries, while the original spatio-temporal visual tokens derived from vision-language models serve as input of their corresponding linear projection layers to deliver keys and values. For each semantic hierarchy, we further incorporate a set of learnable query prompts to increase the query flexibility and thereby improve the generalizability of the model for RAVAR.

The aggregation process is performed at both the spatial and temporal perspectives, where spatial aggregation and temporal aggregation are applied independently prior to the multi-hierarchical

semantic-aligned cross-attention module. Finally, a bounding box regression head and a classification head are applied separately to the spatial and temporal branches. The outputs from both branches are then averaged at the task-head level to produce the final prediction.

Through our experiments, we find that our proposed RefAtomNet++ achieves state-of-the-art performances on both the RefAVA dataset [38] and our new proposed RefAVA++ dataset, demonstrating superior RAVAR performance. RefAtomNet++ consistently outperforms RefAtomNet on RefAVA, boosting test-set scores by +6.10% mIoU, +2.29% mAP, and +1.77% AUROC, while RefAtomNet++ reduces the number of parameters by 93M when comparing with RefAtomNet. With an XCLIP backbone [42], RefAtomNet++ boosts test performance over RefAtomNet from 36.61%→42.24% mIoU, 48.59%→53.03% mAP, and 66.47%→70.50% AUROC, also surpassing the XCLIP encoder [42] alone. The newly proposed mechanism helps the model to understand the scene from a multi-hierarchical semantic perspective, which benefits the visual-textual alignment to reason the fine-grained actions of a desired person. The main contributions of this paper can be summarized as follows.

- In this work, we propose a novel dataset for the RAVAR task, *i.e.*, RefAVA++, which results in 2,950,830 annotated frames and 75,111 annotated persons. This contribution is important as its large scale enables robust training and evaluation for fine-grained, language-guided action recognition in complex scenarios.
- We establish a comprehensive benchmark for the RAVAR task by evaluating 15 strong baselines spanning action recognition and localization, video question answering, and vision-language retrieval, and our previous work, *i.e.*, RefAtomNet, on the RefAVA++ dataset.
- We propose a new method, *i.e.*, RefAtomNet++. It is built upon a vision-language-model-based multi-modal feature extractor and incorporates a novel multi-trajectory semantic-retrieval Mamba. The proposed new method enables multi-level, semantic-aligned visual token aggregation. Furthermore, a multi-hierarchical semantic-aligned cross-attention mechanism is introduced to achieve the final visual-textual alignment and aggregation. Experiments demonstrate that RefAtomNet++ achieves state-of-the-art performances on both RefAVA and RefAVA++ datasets for the RAVAR task.

The main differences between this work and our previous conference version [38] appeared in the European Conference on Computer Vision (ECCV), 2024, lie in the following points:

- We extend the previous RefAVA dataset into RefAVA++ by adding 38,481 newly annotated instances.
- We extend the previous RefAVA benchmark by examining the performance of baselines and our previous method RefAtomNet on the RefAVA++ dataset.
- We propose a new approach, *i.e.*, RefAtomNet++, where multi-trajectory semantic-retrieval Mamba and a multi-hierarchical semantic-aligned cross-attention mechanism are proposed to deal with the fine-granularity visual-language token aggregation challenge. RefAtomNet++ sets new state-of-the-art performances on both of the RefAVA and RefAVA++ datasets for RAVAR task.

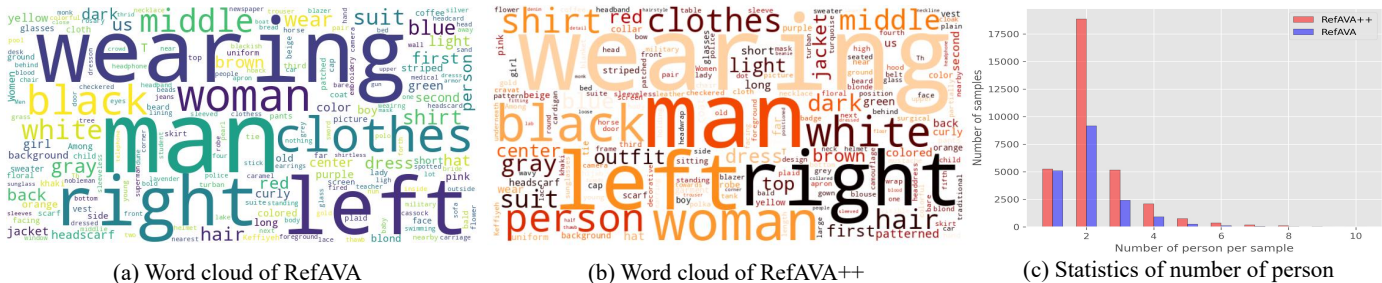


Fig. 2: An overview of the dataset statistics. (a) shows the word cloud of the references from RefAVA, (b) shows the word cloud of the references from RefAVA++, and (c) shows the statistics of the number of annotated persons per sample of RefAVA (blue) and RefAVA++ (red).

TABLE 1: An overview of the referring scene understanding datasets, our previous proposed RefAVA dataset [38], and the proposed RefAVA++ dataset in this work. Our task is Referring Atomic Video Action Recognition (RAVAR), whereas existing benchmarks focus on Referring Object Detection (ROD), Referring Video-based Object Segmentation (RVOS), and Referring Multi-Object Tracking (RMOT).

Dataset	RefCOCO [50]	RefCOCO+ [50]	RefCOCOg [50]	Talk2Car [53]	VID-Sentence [54]	Refer-DAVUS17 [6]	Refer-YV [37]	Refer-KITTI [5]	RefAVA	RefAVA++
Task	ROD	ROD	ROD	ROD	ROD	RVOS	RMOT	RMOT	RAVAR	RAVAR
$N_{Frames}$	26,711	19,992	26,711	9,217	59,238	4,219	93,869	6,650	1,615,140	2,950,830
$N_{Instance}$	26,711	19,992	26,711	10,519	7,654	3,978	7,451	-	36,630	75,111

## 2 RELATED WORK

**Referring Scene Understanding.** Referring scene understanding [43], [44], [45], [46] aims to localize regions or entities of interest within images or videos based on natural language descriptions, and has demonstrated significant utility in a wide range of computer vision applications, such as autonomous driving [5], [47] and video editing [48]. The advancement of this field has been largely driven by the availability of high-quality open-source datasets and benchmarks [5], [6], [10], [12], [49], [50], [51], [52], which provide the foundation for method development and fair evaluation. For instance, the CLEVR-Ref+ benchmark introduced by Liu *et al.* [3] facilitates visual reasoning with referring expressions, while Li *et al.* [8] addressed referring image segmentation through a recurrent refinement network. More recently, Wu *et al.* [5] proposed a benchmark for referring multi-object tracking, extending the scope of referring understanding tasks into dynamic scenarios.

Despite advances in referring scene understanding, prior work has not addressed atomic video action analysis, which requires both spatial localization and fine-grained temporal reasoning. To fill this gap, our earlier study [38] introduced the RefAVA dataset and the first benchmark for Referring Atomic Video Action Recognition (RAVAR). Unlike Referring Video Object Segmentation (RVOS) [45], [55], [56], [57], where references often include explicit action cues, RAVAR demands inferring atomic actions of a referred individual from natural language alone, making alignment of spatial, temporal, and semantic cues particularly challenging. In this work, we extend RAVAR with the RefAVA++ dataset and propose RefAtomNet++, which combines multi-hierarchical semantic-aligned cross-attention mechanism with multi-trajectory semantic-retrieval Mamba modeling, achieving state-of-the-art accuracy and efficiency on both RefAVA [38] and RefAVA++.

**Video Text Retrieval.** Video-Text Retrieval (VTR) aligns videos with natural language by retrieving the most relevant video or text. With large-scale vision-language models such as CLIP [58] and BLIP [59], recent works [39], [42], [60], [61], [62], [63],

[64], [65], [66], [67] adapt these pre-trained representations for retrieval. For example, CLIP4CLIP [61] extended CLIP to videos, XCLIP [42] modeled multi-level correspondences, MeVTR [62] emphasized event-level semantics, and BLIPv2 [39] introduced QFormer for versatile vision-language modeling.

While both VTR and RAVAR combine vision and language, they differ in focus: VTR seeks global semantic alignment for ranking, whereas RAVAR requires localized spatio-temporal reasoning to ground and recognize fine-grained human actions. Here, natural language serves not only as a retrieval query but as a supervisory signal to identify and temporally ground the subtle actions of a referred individual, positioning RAVAR closer to fine-grained video-language grounding than conventional VTR.

**Video Question Answering.** Video Question Answering (VQA) [68], [69], [70], [71], [72] aims to answer natural language queries about video content by jointly reasoning over visual, temporal, and linguistic modalities. Factoid VQA [71], [73], [74], [75], [76], [77], [78], [79], [80], [81], [82], [83], [84], [85], [86], [87] focuses on straightforward questions, while inference-oriented VQA [88], [89] and multimodal extensions [83], [90], [91] tackle higher-order reasoning and integrate multiple input streams. Recent efforts [92], [93] also combine large-scale pre-training and LLMs for advanced temporal and causal reasoning.

However, existing VQA approaches typically yield coarse-grained outputs and are not designed to localize fine-grained atomic actions. This limits their use in domains such as human-robot collaboration [17], [18], assistive monitoring, or skill assessment, where precise temporal predictions are crucial. In contrast, RAVAR grounds natural language to specific individuals and jointly recognizes their atomic actions over time, enabling fine-grained spatio-temporal reasoning that extends beyond conventional VQA.

**Atomic Video Action Recognition and Localization.** Atomic video-based action recognition [25], [94] and localization [31] aim to identify fine-grained human movements in single- and multi-person scenarios. Unlike general action recognition, atomic analysis is more detailed and usually posed as a multi-label

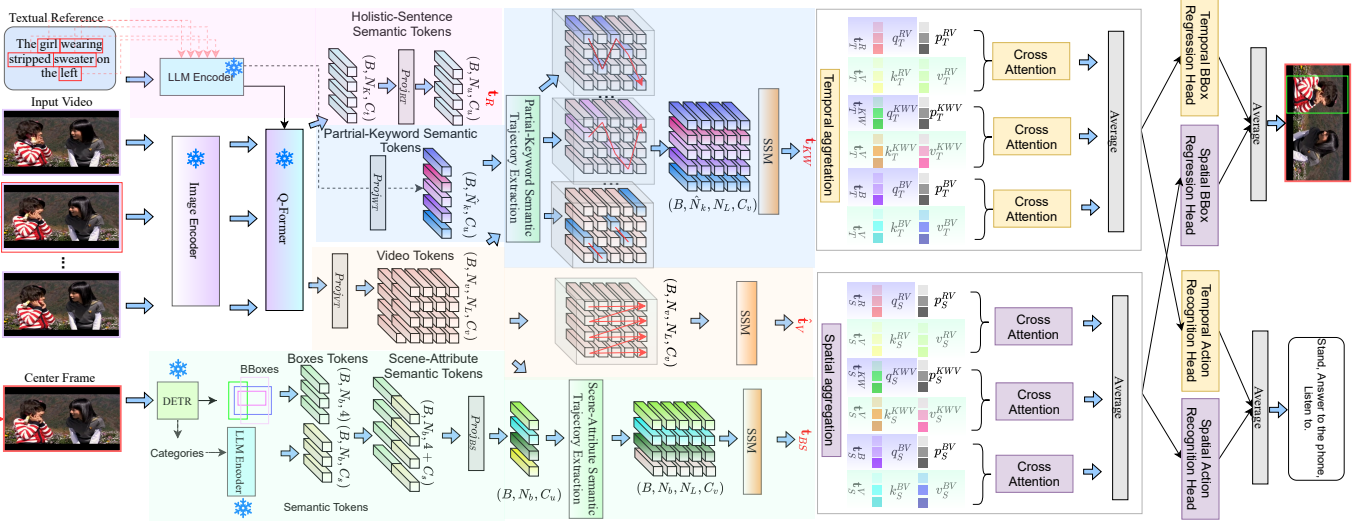


Fig. 3: An overview of the RefAtomNet++. We derive holistic-sentence and partial-keyword semantic tokens using the BLIPv2 LLM Encoder [39], where keywords guide semantic retrieval of the most relevant video tokens per frame to form trajectories for state-space modeling. In parallel, DETR provides bounding-box coordinates concatenated with the corresponding categorical semantics, which also retrieve temporal visual tokens for trajectory construction and are regarded as scene-attribute semantic tokens. These partial-keyword and scene-attribute retrieved trajectories are aggregated by an independent Mamba layer to capture long-range dependencies based on the provided scanning orders. The resulting multi-level semantic-retrieved visual tokens are fused with the original video features via a multi-hierarchical semantic-aligned cross-attention mechanism. Finally, spatial and temporal branches jointly deliver localization and fine-grained action predictions.

problem with bounding boxes to capture concurrent actions. Recent methods employ CNNs [20], [26], [95], [96] and transformers [19], [20], [21], [22], [23], [24], [25], adding classification heads, bounding box regressors, and ROI features; e.g., Ryali *et al.* [19] proposed an efficient hierarchical transformer, and Wang *et al.* [20] improved spatio-temporal learning with dual-masked autoencoders. Yet, vision-only approaches struggle in multi-person settings, often requiring manual cropping or post-hoc selection [33], [97], [98], and cannot address RAVAR. Unlike Atomic Action Localization (AAL), which predicts actions for all individuals, RAVAR tightly integrates natural language grounding with fine-grained spatio-temporal reasoning to directly identify and recognize the referred subject’s actions, posing a more practical and challenging paradigm.

### 3 BENCHMARK

#### 3.1 Introduction of the RefAVA++ dataset

To obtain precise textual annotations for the target individuals, 8 expert annotators were recruited and tasked with providing detailed natural language descriptions based on the key-frame bounding boxes from the AVA dataset [31]. To ensure high annotation quality, a cross-checking process was conducted among annotators, enabling consistency verification and refinement of the textual labels. Discrepant cases were discussed collectively, and only instances that reached clear consensus were retained, while samples with persistent disagreement were discarded. This rigorous protocol ensured both accuracy and linguistic consistency across the dataset, thereby enhancing its reliability for downstream research.

From the AVA dataset, we selected 33,495 video clips spanning 231 movies, with an emphasis on clips that exhibit high visual complexity, diverse environments, and multi-person interactions. Each annotated individual was marked at the center frame of

every clip, ensuring spatial grounding of the textual reference. In total, the RefAVA++ dataset contains 75,111 annotated instances, partitioned into 48,151 for training, 16,142 for validation, and 10,818 for testing.

Of particular importance, the test set comprises 4,566 video clips drawn from 31 movies distinct from those in the training set (150 movies, 21,709 video clips) and validation set (50 movies, 6,513 video clips). This strict movie-level partitioning enforces challenging generalization conditions and provides a reliable setting for evaluating model’s generalizability in diverse and previously unseen environments.

The textual annotations describe salient visual attributes of the referred subjects, including approximate age, gender, clothing style, physical appearance, and relative position in the frame, *etc.* Notably, action descriptions are intentionally excluded to avoid introducing bias toward predefined action categories and to ensure that models learn to infer actions directly from video evidence rather than textual hints.

Dataset statistics are summarized in Tab. 1, where we compare RefAVA++ with representative benchmarks in referring scene understanding. The atomic actions span 80 categories, systematically organized into three groups: Object Manipulation (OM), Person Interactions (PI), and Person Movement (PM). The curated videos capture a wide range of real-world contexts, from everyday interactions to complex multi-person activities.

#### 3.2 Baselines

We implement methods from the general Atomic Action Localization (AAL) field to the Referring Atomic Video Action Recognition (RAVAR) setting by explicitly integrating textual reference embeddings into the visual recognition pipeline according to our previous work [38]. In particular, representative action recognition backbones, *e.g.*, I3D [26] and X3D [95], are reformulated

following the multi-branch procedure outlined in [96]. To encode the natural language references, we employ BERT [99], which provides contextualized textual embeddings that are subsequently fused with the video features for cross-modal reasoning. Since the task requires bounding box localization of the referred subject as part of the output, we remove the cropping operation typically used in conventional AAL pipelines, ensuring that the model learns to both ground the target individual and recognize their actions in a joint framework.

The baselines evaluated span both convolutional and transformer-based paradigms. For CNN-based models, we adopt I3D [26] and X3D [95], which remain strong performances in the spatio-temporal action recognition task. For transformer-based models, we incorporate state-of-the-art architectures including MViTv2 [21], Hiera [19], and VideoMAE [20]. All models are initialized with publicly available pre-trained weights on Kinetics400 [26], thereby providing strong visual priors that facilitate transfer to the RAVAR setting. This design ensures a fair and comprehensive evaluation of different backbone families under the new task formulation, while highlighting the effectiveness of integrating textual grounding into established AAL frameworks.

**VQA Baselines.** The second group of baselines is from the Video Question Answering (VQA) domain, which naturally integrates multi-modal reasoning over video and language. Specifically, we consider a GPT-based model, *i.e.*, AskAnything [93], which leverages large-scale video-text pre-training, and a transformer-based architecture [92] that demonstrates strong performance on diverse VQA tasks. To align these frameworks with the RAVAR setting, we reformulate the textual reference into a question-like format that explicitly queries the identity and actions of the referred subject. To support the dual objectives of RAVAR, we extend the original output layers by appending both a multi-label classification head for atomic action recognition and a bounding box regression head for spatial localization of the referred individual. Both models are fine-tuned end-to-end using their publicly available pre-trained weights from ActivityNetQA [100], ensuring that the strong video-language representations learned from large-scale VQA corpora can be effectively transferred and evaluated under the more fine-grained RAVAR formulation.

**VTR Baselines.** The third group of baselines is drawn from foundation models originally developed for the Video-Text Retrieval (VTR) task, including XCLIP [42], CLIP4CLIP [61], BLIPv2 [39], and MeVTR [62]. These approaches build upon large-scale vision-language pre-training and are trained on diverse video-text and image-text corpora, such as Conceptual Captions [101], SBU Captions [102], and COCO Captions [103], among others, thereby equipping them with strong multi-modal alignment capabilities. To adapt these frameworks to the RAVAR setting, we employ the same reformulation strategy used for the VQA baselines, where the textual reference is treated as a structured query and the model outputs are extended with a multi-label classification head and a bounding box regression head. This adaptation allows us to assess the transferability of retrieval-oriented foundation models to the fine-grained spatio-temporal grounding required by RAVAR. These VTR approaches are selected as baselines because they are well-established foundation models for video-language alignment, allowing us to evaluate how well globally pre-trained retrieval frameworks can transfer to the location estimation and atomic action recognition of the desired person for the RAVAR task.

**SF Baselines.** In addition, we evaluate several Single-Frame

(SF) based foundation model baselines, including SAM [104], DETR [40], and REFLIP [105], each combined with CLIP [58] as the essential cross-modal feature extraction backbone. For these models, key frame-level features are extracted from the respective architectures, aggregated by averaging, and subsequently fed into an action recognition head together with a bounding box regression head, thereby enabling direct prediction of atomic actions and subject localization. These baselines allow us to assess the effectiveness of spatial-only representations without explicit temporal modeling in the RAVAR setting by simply using the combination of existing foundation models.

**VOS Baseline.** In addition, we leverage a Video Object Segmentation (VOS) framework as another baseline by employing the encoder proposed by Su *et al.* [55], which we implement with a task-specific prediction head designed for RAVAR. This modification enables the VOS model, originally developed for pixel-level segmentation, to perform subject grounding and atomic action recognition in a unified manner. Incorporating this baseline further highlights the distinction between segmentation-oriented frameworks and the fine-grained spatio-temporal reasoning required in RAVAR task.

## 4 REFATOMNET++

### 4.1 Background of QFormer

We adopt BLIPv2 [39] as the backbone for visual feature extraction, wherein the Querying Transformer (QFormer) serves as the central component. QFormer introduces a set of learnable queries, initialized as trainable parameters, which interact with the input features through multi-head self-attention and cross-attention mechanisms. Each query selectively attends to different regions of the input representation, enabling the extraction of discriminative and task-relevant features. Through iterative attention interactions, the queries are progressively updated to capture fine-grained semantics and contextual dependencies. During training, these queries are jointly optimized with the network to specialize in extracting complementary aspects of the input, such as spatial context, appearance attributes, and local dynamics. The refined query embeddings are subsequently aggregated and directly employed to generate the final predictions, thereby bridging low-level visual representations with high-level task objectives in a parameter-efficient and semantically aligned manner. This design allows QFormer to function as an adaptive information bottleneck, effectively aligning visual features with the textual reference for downstream tasks.

**Extraction of Visual and Textual Reference Tokens.** We build up our cross-modal feature extractor based on the well-established BLIPv2 approach [39], which leverages the QFormer [39] architecture to effectively extract and integrate multimodal embeddings from the visual data and the textual-reference data. Specifically, the visual branch employs a ViT [106] backbone encoder to process visual inputs, while the textual branch utilizes OPT model [107] to encode textual reference cues. This combined approach facilitates a holistic understanding of both visual content and textual descriptions. The model extracts visual tokens ( $\mathbf{t}_V$ ) and textual reference tokens ( $\mathbf{t}_R$ ) through Eq. 1:

$$\mathbf{t}_V, \mathbf{t}_R = \mathcal{V}_{VL}(\mathcal{V}_{VT}(\mathbf{x}_V), \mathcal{V}_{RT}(\mathbf{x}_R)), \quad (1)$$

where  $\mathcal{V}_{VL}$  represents the visual-textual integration model (*i.e.*, QFormer [39]).  $\mathcal{V}_{VT}$ , and  $\mathcal{V}_{RT}$  denote the backbones for extracting visual tokens (*i.e.*, visual encoder of BLIPv2 [39]) and

textual reference tokens (*i.e.*, textual encoder of BLIPv2 [39]), respectively.  $\mathbf{x}_V$  and  $\mathbf{x}_R$  represent the input video and textual reference caption, which are then fed into linear projection layers, *i.e.*,  $\mathbf{P}_{VT}$  and  $\mathbf{P}_{RT}$ , respectively.

## 4.2 Multi-Trajectory Semantic-Retrieval Mamba

In our previous work, we only considered the semantic embedding from the holistic-sentence perspective, which limits the visual-semantic-retrieval capability for fine-grained action reasoning and thereby results in unsatisfactory RAVAR performances. In this work, we first tackle this challenge through proposing multi-granularity semantic-retrieval token reasoning strategies, where nearest spatial token selection and Mamba-based token trajectory aggregation are proposed and integrated. In total, we take three different semantic hierarchies into consideration, *i.e.*, holistic-sentence-semantic level, partial-keyword-semantic level, and scene-attribute-semantic level.

**Partial-Keyword Trajectory Aggregation (PKTA).** Beyond the holistic-sentence-level reasoning, partial-keyword-level reasoning captures finer semantic details that can further improve the alignment between semantic and visual tokens in finer semantic granularity. Given the textual reference input as Eq. 2,

$$\mathbf{t}_R = \{\mathbf{e}_1, \mathbf{e}_2, \dots, \mathbf{e}_{N_K}\}, \quad \mathbf{e}_i = \mathcal{V}_{RT}(\mathbf{w}_i) \in \mathbb{R}^d, \quad (2)$$

where  $N_K$  denotes the total number of words from the given reference sentence, and  $\mathbf{e}_i$  indicates the semantic embedding of the  $k$ -th word, which has dimension of  $d$ .  $\mathbf{w}_i$  indicates the  $i$ -th original word of the textual reference  $\mathbf{t}_R$ . We first set up a set of stop words, denoted by  $\Omega_{stop}$ . We then mask out all the stop words (*e.g.*, *the*, *a*, *is*, *are*) existing in the textual reference, as Eq. 3.

$$\hat{\mathbf{t}}_R = \mathbf{t}_R / \Omega_{stop}, \quad (3)$$

where  $\hat{\mathbf{t}}_R$  denotes the filtered textual reference. The resultant total number of the keywords after filtering is  $\hat{N}_K$ .

Then, for the semantic embedding of each keyword of  $\hat{\mathbf{t}}_R$ , we retrieve its nearest spatial visual token for each time step, and thereby obtain the desired trajectory of this keyword along the temporal axis. The resultant trajectories are harvested based on all the keywords for a given textual reference. The nearest visual token for each time step can be obtained according to Eq. 4.

$$\mathbf{t}_V^k(l) = \arg \min_{\mathbf{t} \in \mathcal{T}(l)} \|\hat{\mathbf{e}}_k - \mathbf{t}\|, \quad l = [1, \dots, N_L], \quad (4)$$

where  $\hat{\mathbf{e}}_k$  is the  $k$ -th keyword embedding of the reference  $\hat{\mathbf{t}}_R$ ,  $\mathcal{T}(l)$  is the set of spatial-visual tokens at time step  $l$ ,  $\mathbf{t}_V^k(l)$  is the nearest visual token to  $\hat{\mathbf{e}}_k$  at time step  $l$ . Next, we obtain the temporal trajectory of each keyword by Eq. 5.

$$\mathcal{T}_k = \{\mathbf{t}_V^k(1), \mathbf{t}_V^k(2), \dots, \mathbf{t}_V^k(N_L)\}, \quad (5)$$

where  $\mathcal{T}_k$  denotes the trajectory of the  $k$ -th keyword embedding  $\hat{\mathbf{e}}_k$ , and  $N_L$  is the total number of time steps. Finally, we get all the trajectories for all the keywords of the given textual reference by Eq. 6.

$$\mathcal{T}(\hat{\mathbf{t}}_R) = \{\mathcal{T}_1, \mathcal{T}_2, \dots, \mathcal{T}_{\hat{N}_K}\}, \quad (6)$$

where  $\mathcal{T}(\hat{\mathbf{t}}_R)$  represents the set of trajectories for all the keywords.

We then employ Mamba [41] to aggregate the trajectories because its selective-state-space mechanism efficiently captures long-range temporal dependencies while remaining computationally scalable. This allows the model to integrate spatial-semantic

cues along each trajectory into a compact representation that preserves both local dynamics and global context, as Eq. 7. Unlike attention-based aggregation, which performs discrete pairwise weighting, our Mamba-based state-space modeling can be interpreted as learning a continuous-time dynamical system that filters semantic trajectories through recurrent latent transitions. This inductive bias aligns naturally with human action dynamics, where atomic actions evolve smoothly rather than through abrupt framewise changes.

$$\mathbf{t}_{KW} = \text{Mamba}_{KW}(\mathcal{T}(\hat{\mathbf{t}}_R)), \quad (7)$$

where we leverage Mamba [41] to achieve the token aggregation based on the acquired diverse semantic-retrieval trajectories, while the detailed procedure is described as Eq. 8,

$$\begin{aligned} \mathbf{h}_k(l) &= \mathbf{A}_{KW}(\Delta_l) \mathbf{h}_k(l-1) + \mathbf{B}_{KW}(\Delta_l) \mathbf{t}_V^k(l), \\ \mathbf{t}_{KW} &= \mathbf{C}_{KW}(\Delta_l) \mathbf{h}_k(l), \\ l &= [1, \dots, N_L], \quad k = [1, \dots, \hat{N}_K], \end{aligned} \quad (8)$$

where  $\mathbf{t}_V^k(l)$  is the selected visual token on trajectory  $\mathcal{T}_k$  at time step  $l$ ,  $\mathbf{h}_k(l)$  is the hidden state of Mamba, and  $\mathbf{t}_{KW}$  is the aggregated output.  $\mathbf{A}_{KW}(\cdot)$ ,  $\mathbf{B}_{KW}(\cdot)$ ,  $\mathbf{C}_{KW}(\cdot)$  are learnable state-space model kernels, and  $\Delta_l$  is the step size, where we use  $\Delta_l = 1$  for uniform steps. The keyword-semantic-retrieval tokens, *i.e.*,  $\mathbf{t}_{KW}$ , serve as the input to the query projection in our multi-hierarchical semantic-aligned cross-attention mechanism, which will be introduced later.

**Scene-Attribute Trajectory Aggregation (SATA).** Beyond the partial-keyword-semantic trajectory extraction and token aggregation, we introduce a Scene-Attribute Trajectory Aggregation (SATA) module, designed to explicitly capture contextual cues from the surrounding environment that are often neglected when models focus solely on the referred human or textual information. Concretely, we apply an off-the-shelf object detector to the keyframe (*i.e.*, the center frame) of each video clip, and utilize its outputs to extract both bounding box coordinates and semantic embeddings of the detected object categories. These outputs are then transformed into scene-attribute tokens that encode spatial layouts together with semantic context by concatenation along the feature dimension axis, thereby enriching the representation space with complementary scene-level information.

For object detection, we employ the transformer-based DETR [40], which outputs  $N_b$  detection results on the keyframe. The detected instances include both humans and other salient objects with high confidence scores, as formulated in Eq. 9. In this formulation, the bounding box coordinates capture the spatial layout of the scene, while the semantic embeddings provide categorical priors. When combined, these elements form scene-attribute-aware token representations that integrate spatial and semantic context for subsequent reasoning.

$$\mathbf{t}_{boxes}, \mathbf{t}_{cats} = \mathcal{V}_{dets}(\mathbf{x}_k), \quad (9)$$

where  $\mathbf{x}_k$  denotes the keyframe and  $\mathcal{V}_{dets}$  is the detection network. Here,  $\mathbf{t}_{boxes} \in \mathbb{R}^{N_b \times 4}$  are the detected 2D bounding box coordinates (top-left and bottom-right), where  $N_b$  indicates the total number of detected object.  $\mathbf{t}_{cats}$  are the predicted categories of the detected regions in textual form. The category labels are subsequently processed by a text encoder (textual encoder of BLIPv2 [39]) to obtain semantic embeddings.

Scene-attribute tokens are particularly beneficial for the RAVAR task. Many real-world activities are inherently defined not

only by human motion but also by the contextual objects involved (*e.g.*, “answering the phone” cannot be interpreted without the presence of a phone). Incorporating detected scene attributes enables the model to disambiguate visually similar actions by grounding them in their contextual environment. Moreover, spatial configurations of objects often serve as cues of affordances and plausible human-object interactions (*e.g.*, a nearby chair strongly suggests the possibility of “sitting”). Finally, scene attributes provide a stable semantic prior: while motion patterns can vary significantly across instances, object co-occurrence remains more consistent, thereby enhancing retrieval robustness in unconstrained, open-domain scenarios.

We encode both semantic and spatial information by concatenating the semantic embeddings with the bounding box coordinates, followed by a linear projection layer to obtain the scene-attribute tokens, *i.e.*,  $\mathbf{t}_{BS}$ , as defined in Eq. 10.

$$\mathbf{t}_{BS} = \mathbf{P}_{BS}(\text{Concat}[\mathcal{V}_{RT}(\mathbf{r}_{cats}), \mathbf{r}_{boxes}]), \quad (10)$$

where  $\mathbf{P}_{BS}$  is a fully connected layer,  $\mathcal{V}_{RT}$  denotes the language feature extraction backbone, and  $\text{Concat}$  is the concatenation operator. The resulting embeddings  $\mathbf{t}_{BS} = \{\mathbf{b}_1, \mathbf{b}_2, \dots, \mathbf{b}_{N_b}\}$  are then aligned with spatial-visual tokens across time. Specifically, for each detected scene attribute, we retrieve its nearest visual token at each time step to form its corresponding temporal trajectory, as defined by Eq. 11.

$$\tilde{\mathbf{t}}_V^j(l) = \arg \min_{\mathbf{t} \in \mathcal{T}(l)} \|\mathbf{P}_{BS}(\mathbf{b}_j) - \mathbf{t}\|, \quad l = [1, \dots, N_L], \quad (11)$$

where  $\mathbf{b}_j$  is the  $j$ -th scene-attribute token in the keyframe,  $\mathbf{P}_{BS}(\cdot)$  is the linear projection layer,  $\mathcal{T}(l)$  denotes the set of spatial-visual tokens at time step  $l$ , and  $\tilde{\mathbf{t}}_V^j(l)$  is the nearest visual token to  $\mathbf{b}_j$  at timestamp  $l$  for the  $j$ -th recognized object.  $N_b$  is the total number of detected bounding boxes. The temporal trajectory of each detected attribute token is then given by Eq. 12.

$$\mathcal{T}_j^{BS} = \{\tilde{\mathbf{t}}_V^j(1), \tilde{\mathbf{t}}_V^j(2), \dots, \tilde{\mathbf{t}}_V^j(N_L)\}, \quad (12)$$

where  $\mathcal{T}_j^{BS}$  denotes the trajectory of the  $j$ -th scene-attribute token  $\mathbf{b}_j$ . Collectively, the set of trajectories for all detected scene attributes is represented as Eq. 13.

$$\mathcal{T}(\mathbf{t}_{BS}) = \{\mathcal{T}_1^{BS}, \mathcal{T}_2^{BS}, \dots, \mathcal{T}_{N_b}^{BS}\}, \quad (13)$$

where  $\mathcal{T}(\mathbf{t}_{BS})$  indicates the trajectory set for all scene attributes.

Finally, we employ a Mamba scanner to aggregate the trajectories  $\mathcal{T}(\mathbf{t}_{BS})$  into refined temporal representations as Eq. 14.

$$\hat{\mathbf{t}}_{BS} = \text{Mamba}_{BS}(\mathcal{T}(\mathbf{t}_{BS})), \quad (14)$$

where  $\text{Mamba}_{BS}(\cdot)$  is a selective state-space model and  $\hat{\mathbf{t}}_{BS} = \{\hat{\mathbf{t}}_{BS}(1), \dots, \hat{\mathbf{t}}_{BS}(N_L)\}$  are the per-timestep aggregated tokens for the scene-attribute-level reasoning.

**Holistic-Sentence Token Aggregation (HSTA).** Since we adopt the cross-modal feature extractor from the vision-language encoder (*i.e.*, BLIPv2 [39]), the resulting visual tokens inherently incorporate the global semantic context of the entire sentence. To further refine these representations, we employ Mamba [41] to enhance the tokens and obtain holistic-sentence visual-textual aggregation results, formulated as Eq. 15.

$$\hat{\mathbf{t}}_V = \text{Mamba}_V(\mathbf{t}_V), \quad (15)$$

where  $\mathbf{t}_V$  denotes the video token, which is fused with the whole sentence semantic feature from the reference by QFormer.  $\text{Mamba}_V(\cdot)$  is another selective state-space model,  $N_v$  indicates the number of visual tokens, and  $\hat{\mathbf{t}}_V$  are final resultant tokens.

### 4.3 Multi-Hierarchical Semantic-Aligned Cross-Attention Mechanism (MHS-CA)

After obtaining the multi-trajectory semantic-retrieval tokens, we introduce a multi-hierarchical semantic-aligned cross-attention mechanism. This mechanism helps selectively integrate visual tokens and align complementary information between the retrieved tokens and the original visual-language tokens, from both spatial and temporal perspectives. We employ a two-branch architecture that aggregates temporal and spatial information through the proposed multi-hierarchical semantic-aligned cross-attention mechanism separately. Specifically, for each semantic hierarchy, *i.e.*, holistic-sentence-level ( $RV$ ), keyword-level ( $KWV$ ), and scene-attribute-level ( $BV$ ), we concatenate a learnable query embedding  $\mathbf{p}_\alpha^\beta$  with the text-derived query  $\mathbf{q}_\alpha^\beta$  before performing cross-attention, where  $\beta \in \{RV, KWV, BV\}$ , and  $\alpha \in \{T, S\}$  ( $T$  denotes temporal branch and  $S$  denotes spatial branch).

We first conduct feature aggregation for the temporal branch using average pooling along the spatial dimension. For the holistic-sentence semantic-aligned cross-attention module, we use semantic embeddings of the whole textual reference extracted from BLIPv2 [39] textual encoder as the query tokens and query the holistic-sentence retrieved visual tokens, *i.e.*,  $\hat{\mathbf{t}}_V$ . The query tokens  $\mathbf{q}_T^{RV}$  are obtained by applying linear projection on the previously harvested  $\mathbf{t}_R$ , additionally we concatenate learnable queries  $\mathbf{p}_T^{RV}$  with the query tokens to introduce more flexibility of the query and improve the generalizability during training. The key and values tokens, *i.e.*,  $\mathbf{k}_T^{RV}$  and  $\mathbf{v}_T^{RV}$  are acquired through linear projections on  $\hat{\mathbf{t}}_V$ . The whole procedure is described in Eq. 16.

$$\tilde{\mathbf{z}}_T^{RV} = \text{CA}(\text{Concat}[\mathbf{q}_T^{RV}, \mathbf{p}_T^{RV}], \mathbf{k}_T^{RV}, \mathbf{v}_T^{RV}), \quad (16)$$

where  $\text{CA}$  denotes the cross-attention operation and  $\tilde{\mathbf{z}}_T^{RV}$  denotes the aggregated temporal-branch embeddings for holistic-sentence-semantic hierarchy.

Then we conduct a similar procedure as Eq. 17 using the linearly projected partial-keyword semantic-retrieved visual token  $\mathbf{q}_T^{KWV}$  as query, while key and values tokens, *i.e.*,  $\mathbf{k}_T^{KWV}$  and  $\mathbf{v}_T^{KWV}$ , are harvested by linear projections on the holistic-sentence semantic-retrieved visual tokens  $\hat{\mathbf{t}}_V$ .

$$\tilde{\mathbf{z}}_T^{KWV} = \text{CA}(\text{Concat}[\mathbf{q}_T^{KWV}, \mathbf{p}_T^{KWV}], \mathbf{k}_T^{KWV}, \mathbf{v}_T^{KWV}), \quad (17)$$

where  $\mathbf{p}_T^{KWV}$  denotes learnable query prompts for partial-keyword hierarchy.

The scene-attribute-hierarchy semantic-aligned cross attention is achieved by Eq. 18.

$$\tilde{\mathbf{z}}_T^{BV} = \text{CA}(\text{Concat}[\mathbf{q}_T^{BV}, \mathbf{p}_T^{BV}], \mathbf{k}_T^{BV}, \mathbf{v}_T^{BV}), \quad (18)$$

Their average  $\mathbf{z}_T$  is taken as Eq. 19, where  $\text{AVG}$  indicates the mean averaging operation.

$$\mathbf{z}_T = \text{AVG}(\tilde{\mathbf{z}}_T^{RV} + \tilde{\mathbf{z}}_T^{KWV} + \tilde{\mathbf{z}}_T^{BV}). \quad (19)$$

Analogously, for the spatial branch, we obtain according to Eq. 20.

$$\mathbf{z}_S = \text{AVG}(\tilde{\mathbf{z}}_S^{RV} + \tilde{\mathbf{z}}_S^{KWV} + \tilde{\mathbf{z}}_S^{BV}), \quad (20)$$

where  $\tilde{\mathbf{z}}_S^{RV}$ ,  $\tilde{\mathbf{z}}_S^{KWV}$ , and  $\tilde{\mathbf{z}}_S^{BV}$  denote the aggregated spatial tokens for the three aforementioned semantic hierarchies.

The temporal representation  $\mathbf{z}_T$  is forwarded to a bounding box regression head  $\mathbf{f}_T^{\text{reg}}(\cdot)$  and an action recognition head  $\mathbf{f}_T^{\text{cls}}(\cdot)$ , according to Eq. 21.

$$\hat{\mathbf{b}}_T = \mathbf{f}_T^{\text{reg}}(\mathbf{z}_T), \quad \hat{\mathbf{y}}_T = \mathbf{f}_T^{\text{cls}}(\mathbf{z}_T). \quad (21)$$

While the spatial representation  $\mathbf{z}_S$  is passed to their spatial counterparts, according to Eq. 22.

$$\hat{\mathbf{b}}_S = \mathbf{f}_S^{\text{reg}}(\mathbf{z}_S), \quad \hat{\mathbf{y}}_S = \mathbf{f}_S^{\text{cls}}(\mathbf{z}_S), \quad (22)$$

where  $\mathbf{f}_S^{\text{reg}}(\cdot)$  and  $\mathbf{f}_S^{\text{cls}}(\cdot)$  denote another regression head and another classification head, respectively.

Finally, the predictions from temporal and spatial branches are fused by averaging according to Eq. 23.

$$\hat{\mathbf{b}} = \text{AVG}(\hat{\mathbf{b}}_T + \hat{\mathbf{b}}_S), \quad \hat{\mathbf{y}} = \text{AVG}(\hat{\mathbf{y}}_T + \hat{\mathbf{y}}_S), \quad (23)$$

where  $\hat{\mathbf{b}}$  and  $\hat{\mathbf{y}}$  denote the final bounding box and atomic action predictions of the referred person, respectively. Both bounding box regression and action classification inherently require spatial and temporal reasoning, since accurate localization depends on spatial precision as well as temporal consistency, while robust action recognition relies on temporal dynamics contextualized by spatial layouts. By aggregating spatial and temporal features separately and then combining them, the model preserves the distinct contributions of each dimension while enabling richer cross-dimensional cues for both regression and classification.

#### 4.4 Loss Functions

We employ Binary Cross Entropy (BCE) loss for multi-label classification supervision and Mean Squared Error (MSE) loss for bounding box regression supervision, consistent with all baseline approaches. The BCE loss is formulated as in Eq. 24,

$$L_{\text{BCE}}(\mathbf{y}, \hat{\mathbf{y}}) = -\frac{1}{N_c} \sum_{i=1}^{N_c} [\mathbf{y}_i \log(\hat{\mathbf{y}}_i) + (1 - \mathbf{y}_i) \log(1 - \hat{\mathbf{y}}_i)], \quad (24)$$

where  $\mathbf{y}$  denotes the one-hot ground truth vector,  $\hat{\mathbf{y}}$  represents the predicted probabilities, and  $N_c$  is the number of action categories.

For bounding box regression, the MSE loss is defined in Eq. 25,

$$L_{\text{MSE}}(\mathbf{b}, \hat{\mathbf{b}}) = \sum_{j=1}^4 (\mathbf{b}_j - \hat{\mathbf{b}}_j)^2, \quad (25)$$

where  $\mathbf{b}$  represents the ground-truth coordinates of the bounding box (top-left and bottom-right corners),  $\hat{\mathbf{b}}$  denotes the predicted coordinates, and  $j$  indexes the four bounding box parameters.

## 5 EXPERIMENTS

### 5.1 Implementation Details

All experiments are conducted on four NVIDIA A100 GPUs. We employ the BertAdam [108] optimizer with a learning rate  $lr = 1e^{-4}$ , batch size of 128, learning rate decay of 0.9, and a warmup ratio of 0.1. The model is trained for 40 epochs on our dataset. During training, the text encoder, visual encoder, object detector, and QFormer from BLIPv2 [39] are kept frozen. For each level of Mamba-based semantic-visual aggregation, we first adopt a linear projection layer to project the feature dimension from 768 to 256 and then apply a single Mamba layer to achieve the state-space modeling. For evaluation, we adopt multi-label mean Average Precision (mAP), Area Under the Receiver Operating Characteristic (AUROC) curve, and mean Intersection over Union (mIOU) as evaluation metrics.

### 5.2 Analysis of the Benchmark

The results of the experiments on the RefAVA and RefAVA++ datasets are reported in Table 2. We compare the proposed RefAtomNet++ against a broad set of representative baselines adapted to our task, drawn from five research areas: (1) Atomic Action Localization (AAL), (2) Video Question Answering (VQA), (3) Video-Text Retrieval (VTR), (4) Single-Frame (SF) baselines, and (5) Video Object Segmentation (VOS), and our previously proposed framework, *i.e.*, RefAtomNet [38].

**Analysis of the Performances on the RefAVA dataset.** Baselines from the AAL category consistently underperform in spatially localizing the referred person with respect to textual references, as measured by mIOU. I3D [26], X3D [95], MViTv2-B [21], VideoMVAE2-B [20], and Hiera-B [19] obtain 44.04%, 44.45%, 42.32%, 42.02%, and 42.74% mAP on the validation set, and 44.64%, 46.34%, 42.60%, 41.87%, and 41.14% on the test set, respectively. Among them, X3D achieves the highest AUROC with 59.09% (val) and 64.51% (test).

Baselines from VQA and VTR yield stronger results than AAL, as these tasks inherently benefit from text-aware pretraining, enabling them to better capture the referred person while maintaining reasonable action recognition performance. For instance, AskAnything [93] from the VQA group achieves 20.09%/22.35% mIOU, 51.42%/52.25% mAP, and 66.12%/69.35% AUROC on the val/test sets. Similarly, BLIPv2 [59] from the VTR group reports 32.99%/32.75% mIOU, 52.13%/53.19% mAP, and 66.56%/69.92% AUROC.

By contrast, our previous work, *i.e.*, RefAtomNet [38], leverages the proposed cross-stream agent-based location-semantic-aware attentional fusion mechanism to suppress irrelevant visual tokens according to textual references and scenario cues. As a result, it surpasses the best-performing baseline BLIPv2 by margins of 5.23%/3.67% (mIOU), 3.85%/4.33% (mAP), and 3.17%/4.03% (AUROC) on the val/test sets.

By taking multi-hierarchical semantic information into consideration during the visual-language alignment, our new model RefAtomNet++ achieves state-of-the-art performances and outperforms RefAtomNet by 5.49%/6.10% (mIOU), 0.85%/2.29% (mAP), 1.54%/1.77% (AUROC) on the val/test sets, respectively. The superior performance of RefAtomNet++ primarily stems from its model design, which integrates state-space modeling to perform smooth, memory-efficient multi-semantic trajectory aggregation and thus captures long-range temporal dependencies among atomic actions. Moreover, the proposed multi-hierarchical semantic-aligned cross-attention enables complementary interaction between holistic, keyword, and scene-level cues, allowing the model to achieve finer visual-language alignment and more discriminative reasoning compared to conventional attention-based baselines.

**Analysis of the performances on the RefAVA++ dataset.** First, we can still observe that the baselines adopted from the AAL domain fail to localize the desired referred person precisely due to the lack of visual-language alignment capability obtained through the pretraining stage. Among all the transformer-based approaches, MViTv2-B [21] achieves the best performance by delivering 0.07%/0.11% (mIOU), 48.16%/48.16% (mAP), and 64.21%/63.66% (AUROC) on the val/test sets. X3D [95] achieves the best performances among all the CNN-based AAL approaches by providing 8.91%/9.03% (mIOU), 44.16%/44.57% (mAP), and 58.74%/59.87% (AUROC) on the val/test sets.

TABLE 2: Experimental results on both the RefAVA dataset and the RefAVA++ dataset. Approaches are evaluated using mIOU for referred person localization, mAP and AUROC for referred person atomic action recognition. Performances of the validation set (Val) and test set (Test) on these two datasets are reported.  $N_p$  indicates the number of parameters.

Dataset			RefAVA						RefAVA++					
Method		# $N_p$	mIOU	mAP	AUROC									
			Val			Test			Val			Test		
AAL	I3D [26]	25M	0.00	44.04	57.77	0.00	44.64	62.71	0.00	44.13	58.79	0.00	45.26	60.03
	X3D [95]	3.76M	0.26	44.45	59.09	0.27	46.34	64.51	8.91	44.16	58.74	9.03	44.57	59.87
	MViTv2-B [21]	71M	0.76	42.32	56.43	0.66	42.60	59.30	0.07	48.16	64.21	0.11	48.16	63.66
	VideoMAE2-B [20]	87M	0.16	42.02	55.12	0.29	41.87	59.10	0.14	43.46	58.73	0.09	43.76	58.76
	Hiera-B [19]	52M	0.49	42.74	56.72	0.62	41.14	58.70	0.52	45.45	60.90	0.50	46.11	60.90
VQA	Singularity [92]	203M	26.34	42.43	59.52	29.78	42.18	56.12	27.26	41.14	55.60	25.30	42.76	57.50
	AskAnything13B [93]	0.66M	20.09	51.42	66.12	22.35	52.25	69.35	27.43	42.36	56.98	26.30	44.60	58.96
VTR	MeVTR [62]	164M	30.78	38.42	51.01	29.79	36.27	52.45	29.02	38.24	52.62	29.15	38.24	51.52
	CLIP4CLIP [61]	149M	34.75	39.48	52.57	32.33	37.17	55.05	35.07	40.22	54.03	34.20	40.37	53.89
	XCLIP [42]	150M	35.54	42.46	56.30	31.79	40.82	58.71	36.26	51.37	67.15	35.80	51.37	67.15
	BLIPv2 [39]	187M	32.99	52.13	66.56	32.75	53.19	69.92	23.50	54.58	70.16	23.40	54.75	70.22
SF	CLIP [58]+SAM [104]	241M	32.95	49.74	64.55	29.80	51.34	69.11	22.34	55.77	70.51	22.41	53.82	69.41
	CLIP [58]+DETR [40]	167.8M	33.96	47.57	61.83	33.84	50.92	67.29	28.80	51.52	66.70	27.09	48.65	64.15
	CLIP [58]+REFCLIP [105]	213M	34.43	47.79	62.50	32.28	49.90	67.44	29.44	50.69	65.72	30.78	51.07	66.33
VOS	<i>Su et al.</i> [55]	67M	23.71	52.17	66.67	26.02	53.20	70.19	28.91	52.35	67.49	28.07	51.47	67.06
	RefAtomNet	214M	38.22	55.98	69.73	36.42	57.52	73.95	35.97	56.54	70.97	35.73	57.01	71.62
	RefAtomNet++	121M	<b>43.71</b>	<b>56.83</b>	<b>71.27</b>	<b>42.52</b>	<b>59.81</b>	<b>75.72</b>	<b>39.12</b>	<b>58.24</b>	<b>72.58</b>	<b>38.58</b>	<b>58.84</b>	<b>73.28</b>

TABLE 3: Experimental results for module ablation of RefAtomNet++ on the RefAVA dataset.

Method	mIOU	mAP	AUROC	mIOU	mAP	AUROC
	Val			Test		
BLIPv2 [39]	32.99	52.13	66.56	32.75	53.19	69.92
w/o TSR-QB	36.93	55.41	69.63	36.93	59.47	74.79
w/o BSR-QB	38.97	55.72	69.84	38.60	58.08	73.76
w/o T-QB	27.14	54.82	69.14	29.00	56.83	73.29
w/o MHS-CA	39.19	55.22	69.43	36.84	56.53	73.97
w/o QPrompts	43.33	55.52	69.72	41.40	58.50	75.13
Ours	<b>43.71</b>	<b>56.83</b>	<b>71.27</b>	<b>42.52</b>	<b>59.81</b>	<b>75.72</b>

TABLE 4: Ablation of temporal and spatial reasoning branches of RefAtomNet++ on the RefAVA dataset.

Method	mIOU	mAP	AUROC	mIOU	mAP	AUROC
	Val			Test		
BLIPv2 [39]	32.99	52.13	66.56	32.75	53.19	69.92
w/o TA	40.51	55.71	70.15	39.81	57.91	74.33
w/o SA	40.40	55.37	69.95	39.31	57.66	74.53
Ours	<b>43.71</b>	<b>56.83</b>	<b>71.27</b>	<b>42.52</b>	<b>59.81</b>	<b>75.72</b>

TABLE 5: Ablation studies on different trajectory aggregation strategies. The experiments are conducted on the RefAVA dataset.

Method	mIOU	mAP	AUROC	mIOU	mAP	AUROC
	Val			Test		
LSTM	38.43	55.54	69.73	37.05	57.32	74.45
Linear Projection	36.00	55.51	69.89	34.83	58.09	74.44
Transformer	39.46	55.64	69.98	39.06	58.35	74.76
Ours	<b>43.71</b>	<b>56.83</b>	<b>71.27</b>	<b>42.52</b>	<b>59.81</b>	<b>75.72</b>

Among all the VQA baselines, AskAnything13B [93] achieves performances of 27.43%/26.30% (mIOU), 42.36%/44.60% (mAP), and 56.98%/58.96% (AUROC) on the val/test sets, respectively. Among all the VTR baselines, XCLIP [42] harvests the best localization performance by 36.26%/35.80% (mIOU) while BLIPv2 [39] shows the best fine-grained action recognition performance for the referred person by delivering 54.58%/54.75%

TABLE 6: Comparison with other multi-modal fusion strategies on the RefAVA dataset.

Fusion	mIOU	mAP	AUROC	mIOU	mAP	AUROC
	Val			Test		
Addition	27.30	50.70	65.31	29.09	51.26	68.20
Concatenation	18.64	52.23	66.45	20.65	53.44	70.70
Multiplication	23.90	51.55	65.66	25.05	53.33	70.48
AttentionBottleneck [109]	33.47	50.97	65.07	33.02	54.02	71.08
McOmet [110]	23.88	51.58	65.65	25.02	53.21	70.42
RefAtomNet	38.22	55.98	69.73	36.42	57.52	73.95
RefAtomNet++	<b>43.71</b>	<b>56.83</b>	<b>71.27</b>	<b>42.52</b>	<b>59.81</b>	<b>75.72</b>

TABLE 7: Experimental results on test-time rephrasing. The experiments are conducted on the RefAVA dataset.

Method	mIOU	mAP	AUROC	mIOU	mAP	AUROC
	Val			Test		
Singularity [92]	18.45	41.27	58.47	20.54	41.39	55.32
XCLIP [42]	31.95	41.35	54.35	29.84	40.74	58.45
AskAnything [93]	19.74	51.11	65.83	21.60	51.96	69.04
BLIPv2 [39]	31.00	51.45	65.88	31.34	52.35	68.87
RefAtomNet	34.65	55.75	69.52	33.14	57.23	73.76
RefAtomNet++	<b>40.07</b>	<b>57.10</b>	<b>71.54</b>	<b>39.67</b>	<b>58.82</b>	<b>75.26</b>

TABLE 8: Generalizability to different visual-textual encoder architectures. The experiments are conducted on the RefAVA dataset.

Method	mIOU	mAP	AUROC	mIOU	mAP	AUROC
	Val			Test		
XCLIP [42]	35.54	42.46	56.30	31.79	40.82	58.71
RefAtomNet (XCLIP)	38.59	47.40	61.20	36.61	48.59	66.47
RefAtomNet++ (XCLIP)	<b>44.12</b>	<b>53.45</b>	<b>67.55</b>	<b>42.24</b>	<b>53.03</b>	<b>70.50</b>
BLIPv2 [39]	32.99	52.13	66.56	32.75	53.19	69.92
RefAtomNet (BLIPv2)	38.22	55.98	69.73	36.42	57.52	73.95
RefAtomNet++ (BLIPv2)	<b>43.71</b>	<b>56.83</b>	<b>71.27</b>	<b>42.52</b>	<b>59.81</b>	<b>75.72</b>

(mAP), and 70.16%/70.22% (AUROC) on the val/test sets, respectively.

Among all the SF baselines, the combination of features from CLIP [58]+RefCLIP [105] achieves the best localization performance for the desired person by 29.44%/30.78% (mIOU) while the combination of CLIP [58]+SAM [104] achieves the best fine-grained action recognition for the de-

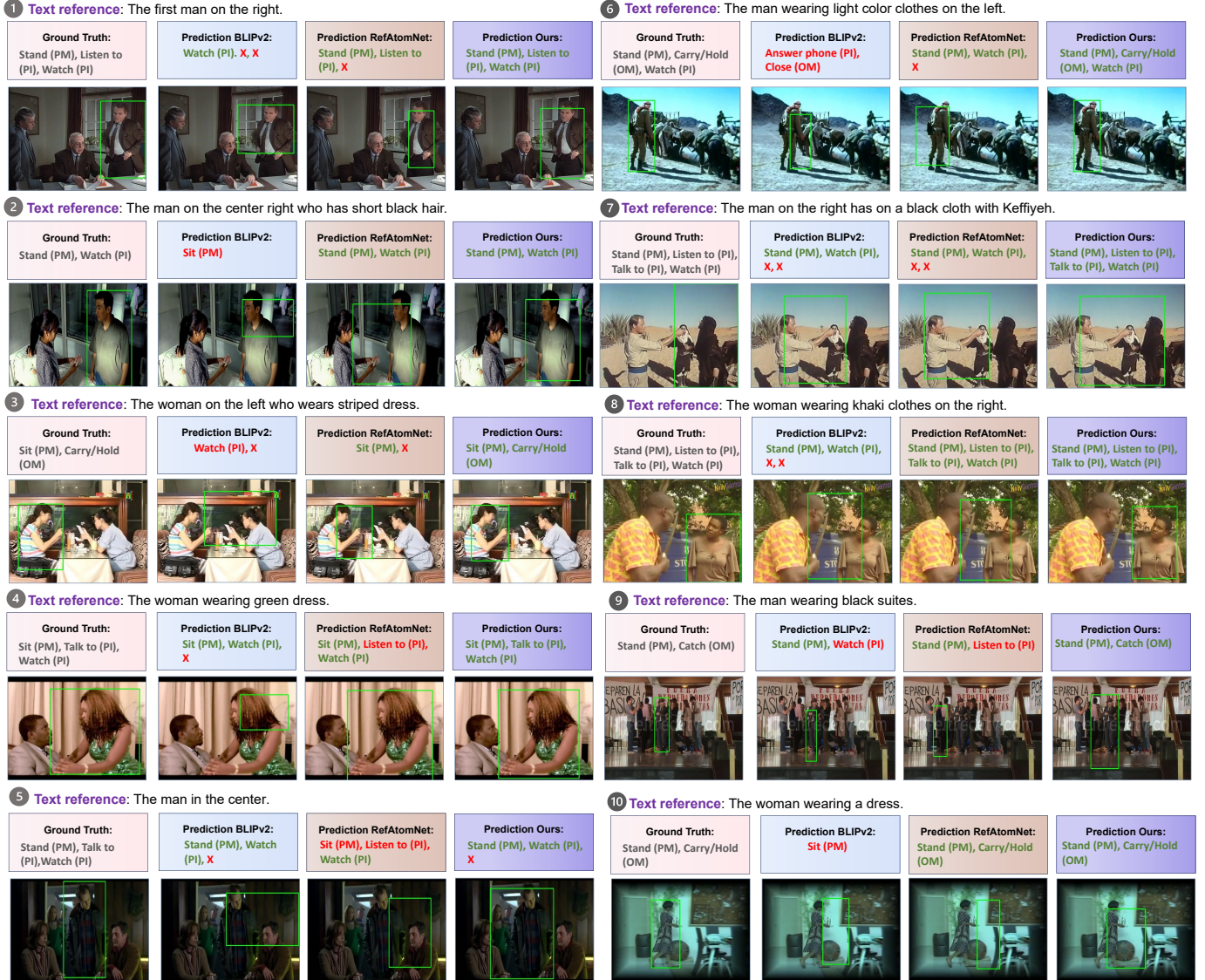


Fig. 4: Qualitative comparisons of BLIPv2 [39], RefAtomNet, and RefAtomNet++ on the RefAVA test set. Each row shows a textual reference, the corresponding ground truth actions, and predictions from the three models. RefAtomNet++ consistently localizes the correct referred individual and predicts fine-grained atomic actions more accurately, while BLIPv2 [39] and RefAtomNet often confuse subjects or miss critical actions, especially in cluttered multi-person scenarios.

TABLE 9: Generalizability to other object detectors. The experiments are conducted on the RefAVA dataset.

Method	mIOU	mAP	AUROC	mIOU	mAP	AUROC
	Val	Test				
BLIPv2 [39]	32.99	52.13	66.56	32.75	53.19	69.92
RefAtomNet (RetinaNet [111])	38.65	55.08	69.16	37.82	56.67	73.63
RefAtomNet (DETR [40])	38.22	55.98	69.73	36.42	57.52	73.95
RefAtomNet++ (RetinaNet [111])	41.65	56.04	70.34	40.06	<b>59.85</b>	75.44
RefAtomNet++ (DETR [40])	<b>43.71</b>	<b>56.83</b>	<b>71.27</b>	<b>42.52</b>	59.81	<b>75.72</b>

sired person by 55.77%/53.82% (mAP), and 70.51%/69.41% (AUROC) on the val/test sets, respectively. Additionally, the baseline comes from the VOS field, *i.e.*, Su *et al.* [55], achieves 28.91%/28.07% (mIOU), 52.35%/51.47% (mAP), and 67.49%/67.06% (AUROC) on the val/test sets. Our previously proposed approach, *i.e.*, RefAtomNet, harvests 35.97%/35.73% (mIOU), 56.54%/57.01% (mAP), and 70.97%/71.62% (AUROC) on the val/test sets of RefAVA++, which illustrates the strong performance of the cross-stream agent attention fusion

TABLE 10: Ablation study on the number of learnable queries conducted on the RefAVA dataset.

#Queries	mIOU	mAP	AUROC	mIOU	mAP	AUROC
	Val	Test				
2	39.70	56.65	70.71	41.34	59.31	75.13
4	42.75	56.69	71.22	42.20	<b>59.83</b>	<b>76.07</b>
6	<b>43.71</b>	<b>56.83</b>	<b>71.27</b>	<b>42.52</b>	59.81	75.72
8	42.90	56.41	70.86	41.88	59.35	75.37
10	42.31	56.55	70.95	41.30	59.51	75.37
12	41.60	56.48	70.81	40.55	59.69	75.55

for suppressing useless tokens in the RAVAR task. On the other hand, our new proposed RefAtomNet++ from this work sets new state-of-the-art performances by 39.12%/38.58% (mIOU), 58.24%/58.84% (mAP), and 72.58%/73.28% (AUROC) on the val/test sets, respectively. RefAtomNet++ advances the RAVAR task due to several reasons. First, we introduce multi-trajectory semantic-retrieval Mamba modeling, which dynamically constructs semantic-aligned visual trajectories at the partial-keyword,

TABLE 11: Ablation of the frame number. The experiments are conducted on the RefAVA dataset.

#Frames	mIOU			mAP			AUROC		
	Val			Test					
2	36.02	55.87	69.97	35.11	59.33	74.76			
4	39.32	56.39	70.59	38.66	60.06	75.18			
6	42.10	56.71	71.18	41.33	<b>60.16</b>	75.63			
8	<b>43.71</b>	<b>56.83</b>	<b>71.27</b>	<b>42.52</b>	59.81	<b>75.72</b>			
10	42.51	56.74	71.19	41.58	60.07	75.60			
12	42.04	56.74	71.20	41.21	60.13	75.63			

scene-attribute, and holistic-sentence semantic levels, enabling efficient long-range dependency modeling while filtering irrelevant tokens. Second, the multi-hierarchical semantic-aligned cross-attention mechanism fuses these multi-level semantic tokens with spatio-temporal visual features, strengthening fine-grained visual-textual alignment for precise action grounding. Third, by jointly modeling spatial and temporal branches with separate regression and classification heads, the framework effectively captures both localization and atomic action dynamics. Finally, leveraging a strong vision-language backbone, *i.e.*, BLIPv2 [39], ensures robust multimodal feature extraction, while Mamba-based aggregation keeps the approach computationally efficient compared to other methods.

### 5.3 Module Ablations

**Analysis of each component.** Table 3 reports the ablation experiments conducted by removing individual semantic levels from the proposed semantic-visual retrieval aggregation. Specifically, *w/o TSR-QB* denotes the removal of the partial-keyword semantic-retrieved Mamba together with its associated semantic-aligned cross-attention module of our RefAtomNet++. Similarly, *w/o BSR-QB* refers to discarding the scene-attribute semantic-retrieved Mamba and its corresponding semantic-aligned cross-attention component, while *w/o T-QB* indicates the exclusion of the holistic-sentence semantic-retrieval Mamba and its corresponding semantic-aligned cross-attention mechanism for reasoning. Additionally, we provide the experiments by removing all the learnable query prompts for each hierarchy of the semantic-aligned cross-attention to examine the efficacy of the design of this component.

Compared to the full model, *i.e.*, RefAtomNet++, all ablated variants exhibit clear performance degradation, confirming the complementary role of multi-level semantic aggregation. Specifically, removing the keyword-level retrieval (*w/o TSR-QB*) reduces the mIoU from 43.71% to 36.93% and mAP from 56.83% to 55.41% on the validation set, highlighting the importance of fine-grained textual cues. Furthermore, the absence of scene-attribute semantic hierarchy (*w/o BSR-QB*) leads to a decline in mIoU (from 43.71% to 38.97%) and AUROC (from 71.27% to 69.84%) on the validation set, showing the importance of the alignment cues provided by the scene-attribute hierarchy.

The most severe drop is observed when removing holistic textual alignment (*w/o T-QB*), where mIoU drops sharply to 27.14%/29.00% and mAP drops to 54.82%/56.83% on val/test sets, indicating that holistic semantic-textual alignment is critical for providing sufficient information from either foreground perspective and background perspective. Removing learnable query prompts (*w/o QPrompts*) also weakens the performance of RefAtomNet++. Learnable query prompts help RefAtomNet++ by increasing the flexibility of feature learning and improving generalization in aligning textual seman-

tics with spatio-temporal visual tokens. Overall, our complete RefAtomNet++ achieves the best performance on both validation and test sets, surpassing all ablated variants. We also deliver the ablation variant by removing the Multi-Hierarchical Semantic-aligned Cross Attention (*w/o MHS-CA*), where we observe a large performance decay of RAVAR, especially towards the localization capability of the referred person. Our approach outperforms this variant by 4.52%/5.68% (mIoU), 1.61%/3.28% (mAP), 1.84%/1.75% (AUROC) on RefAVA val/test sets, respectively. This observation turns out that the MHS-CA contributes to multi-granularity visual-language reasoning by applying queries from different semantic hierarchies, which benefits RefAtomNet++ by providing nuanced and well-aligned visual-language cues.

**Analysis of ablation experiments regarding the temporal and spatial aggregation branch.** Table 4 reports ablation results of RefAtomNet++ on the RefAVA dataset by individually removing the temporal and spatial reasoning branches. Without the temporal aggregation branch (*w/o TA*), performance drops from 42.52% to 39.81% mIoU and from 59.81% to 57.91% mAP on the test set, indicating that temporal reasoning is critical for capturing motion cues and action continuity. Similarly, removing the spatial aggregation branch (*w/o SA*) reduces mIoU to 39.31% and mAP to 57.66%, showing the importance of spatial reasoning for precise localization of the referred individual and the prediction of the atomic-level actions. While both branches contribute significantly, their joint integration yields the best results, with RefAtomNet++ achieving 42.52% mIoU, 59.81% mAP, and 75.72% AUROC on the test set, outperforming all the variants.

**Analysis of different trajectory aggregation methods.** Table 5 reports ablation results on different strategies for semantic trajectory aggregation. Compared to LSTM, Linear Projection, and Transformer variants, our Mamba-based approach consistently achieves the best results across all metrics and sets. Specifically, it improves validation mIoU by +4.25% over the best baseline (Transformer) and test mIoU by +3.46%, showing stronger spatial grounding ability. On action recognition, Mamba also outperforms alternatives, reaching 56.83%/59.81% mAP on val/test, surpassing Transformer’s 55.64%/58.35%. AUROC follows the same trend, with Mamba achieving 71.27%/75.72%, again higher than all baselines. These results highlight that the selective state-space modeling of Mamba better captures long-range temporal dependencies and integrates semantic cues, making it more effective for fine-grained RAVAR. State-space modeling offers a continuous and memory-efficient way to aggregate semantic trajectories by capturing long-range temporal dependencies with stable dynamics. Unlike the other ablated counterparts, it enables smooth temporal filtering and considers coherent visual-semantic cues from different hierarchies that ensure a better alignment between the given textual reference and motion cues of the desired person.

**Comparison with other multi-modal fusion strategies.** Table 6 presents a comparison of RefAtomNet++ against alternative multi-modal fusion strategies on the RefAVA dataset. Simple fusion methods such as addition, concatenation, and multiplication perform poorly, with validation and test mIoU scores below 27.30% and 29.09%, respectively, reflecting their inability to capture complex cross-modal dependencies. More sophisticated approaches, including AttentionBottleneck [109] and McOmet [110], achieve better results but still lag behind RefAtomNet, with 36.42% mIoU, 57.52% mAP, and 73.95% AUROC on the test set. In contrast, RefAtomNet++ establishes

a new state-of-the-art with 42.52% mIoU, 59.81% mAP, and 75.72% AUROC on the test set, surpassing all fusion baselines by a substantial margin. This improvement stems from its multi-hierarchical semantic-aligned cross-attention and multi-trajectory Mamba-based aggregation, which enables more effective fine-grained alignment of textual and visual cues across spatial and temporal dimensions from holistic-sentence, partial-keyword, and scene-attribute perspectives.

#### Analysis of the generalizability towards test-time rephrasing.

Table 7 presents the experimental results under the challenging setting of test-time rephrasing, where each textual query is rephrased three times using ChatGPT [112] and the averaged performance is reported. This setting evaluates model robustness to linguistic variations, a critical aspect for practical deployment in natural human-computer interaction scenarios. Existing multimodal baselines, including Singularity [92], XCLIP [42], AskAnything [93], and BLIPv2 [39], show considerable sensitivity to rephrasing, with mIoU values dropping below 31.34% on the test set. RefAtomNet demonstrates improved robustness, maintaining 33.14% mIoU, 57.23% mAP, and 73.76% AUROC despite the linguistic shifts. RefAtomNet++ achieves the best overall results, boosting performance to 39.67% mIoU, 58.82% mAP, and 75.26% AUROC on the test set. These results highlight the effectiveness of our multi-trajectory semantic-retrieval Mamba and multi-hierarchical semantic-aligned cross-attention design in mitigating the adverse effects of query reformulation, thereby enabling more reliable RAVAR under natural language variability.

**Analysis of the generalizability to different visual-textual encoders.** Table 8 presents the evaluation of RefAtomNet++ with different visual-textual encoder architectures to assess its generalizability. Using both XCLIP [42] and BLIPv2 [39], RefAtomNet++ consistently outperforms the corresponding RefAtomNet baselines as well as the backbone encoders alone. For instance, with the XCLIP encoder, RefAtomNet++ improves mIoU from 36.61% to 42.24%, mAP from 48.59% to 53.03%, and AUROC from 66.47% to 70.50% on the test set. Similarly, with BLIPv2, it achieves significant gains, raising mIoU from 36.42% to 42.52%, mAP from 57.52% to 59.81%, and AUROC from 73.95% to 75.72%. RefAtomNet++ generalizes well across different vision-language backbones because its multi-trajectory semantic-retrieval and multi-hierarchical cross-attention modules provide a flexible fusion mechanism from different semantic hierarchies that complements and enhances diverse encoder representations.

**Analysis of the generalizability towards different object detectors.** Table 9 evaluates the generalizability of RefAtomNet++ across different object detectors, comparing RetinaNet [111] and DETR [40]. As shown, both RefAtomNet and RefAtomNet++ outperform the BLIPv2 [39] baseline regardless of the underlying detector, indicating that our framework is not tied to a specific detection backbone. With RetinaNet, RefAtomNet++ achieves 40.06% mIoU, 59.85% mAP, and 75.44% AUROC on the test set, already surpassing RefAtomNet with the same detector. When coupled with DETR, performance further improves to 42.52% mIoU, 59.81% mAP, and 75.72% AUROC, representing the best overall results. These findings demonstrate that the proposed semantic-retrieval Mamba and multi-hierarchical semantic-aligned cross-attention design of RefAtomNet++ remains effective across different detection paradigms, confirming its robustness and adaptability in diverse visual grounding pipelines.

**Analysis of the ablation for learnable queries.** Table 10 reports

the ablation study on the number of learnable queries used in RefAtomNet++. We vary the query number from 2 to 12. Using too few queries (e.g., 2) leads to insufficient learnable flexibility, while too many queries (e.g., 10 or 12) result in redundancy and diluted attention, both causing degraded performance. The best trade-off is achieved with 6 queries, where RefAtomNet++ obtains the highest overall scores of 43.71% mIoU, 56.83% mAP, and 71.27% AUROC on the validation set and 42.52% mIoU, 59.81% mAP, and 75.72% AUROC on the test set. These results suggest that an intermediate query number offers a balanced capacity to capture fine-grained action correspondences while avoiding over-fragmentation of attention.

#### Analysis of the ablation for the number of temporal frames.

Table 11 presents the ablation study for the number of frames sampled per video on RefAtomNet++. We experiment with frame counts ranging from 2 to 12 and observe that both very short clips and overly long clips lead to suboptimal results. Using only 2 or 4 frames fails to capture sufficient temporal context, while extending to 10 or 12 frames introduces redundancy and noise, slightly degrading performance. The optimal balance is achieved with 8 frames, where the model reaches the best trade-off between spatial-temporal coverage and efficiency. This demonstrates that moderate temporal sampling provides enough motion cues for fine-grained action reasoning without overwhelming the cross-modal alignment process.

## 5.4 Analysis of the Qualitative Results

Figure 4 illustrates qualitative comparisons among BLIPv2 [39], RefAtomNet, and our proposed RefAtomNet++ in diverse multi-person scenarios. In structured indoor settings (examples 1–5), BLIPv2 often misidentifies the referred individual or omits key actions, while RefAtomNet shows improvements but still struggles with compound or fine-grained distinctions. In contrast, RefAtomNet++ consistently grounds the correct subject and accurately covers subtle or multi-action cases. For challenging outdoor (examples 6–8, 10) and crowded (example 9) scenes, BLIPv2 produces spurious predictions and RefAtomNet suffers from misalignments, whereas RefAtomNet++ remains robust, correctly disambiguating references and capturing full action sets. These gains stem from its multi-hierarchical trajectory Mamba, which dynamically aggregates partial-keyword-, scene-attribute-, and holistic-sentence-level cues to filter irrelevant tokens, strengthen long-range temporal reasoning, and adaptively emphasize semantically aligned visual evidence. As a result, RefAtomNet++ achieves more reliable grounding and fine-grained action recognition in complex real-world conditions.

## 6 CONCLUSION

In this work, we introduced RefAVA++, a large-scale benchmark for Referring Atomic Video Action Recognition (RAVAR) with  $> 2.9$  million frames and  $> 75.1k$  annotated persons, extending our earlier RefAVA dataset. Benchmarking across multiple baselines highlights the core challenges of RAVAR, accurately localizing the referred individual and recognizing their fine-grained actions under natural language guidance. To address this, we proposed RefAtomNet++, which combines semantic-retrieval, Mamba-based visual token enhancement, and multi-hierarchical semantic-aligned cross-attention mechanism for improved cross-modal alignment. Experiments on RefAVA and RefAVA++ demonstrate that RefAtomNet++ achieves state-of-the-art performance in complex multi-person scenarios.

## ACKNOWLEDGMENTS

The project is funded by the Deutsche Forschungsgemeinschaft (DFG, German Research Foundation) – SFB 1574 – 471687386. This work is also supported in part by the SmartAge project sponsored by the Carl Zeiss Stiftung (P2019-01-003; 2021-2026), the University of Excellence through the “KIT Future Fields” project, in part by the Helmholtz Association Initiative and Networking Fund on the HoreKA@KIT partition and the state of Baden-Württemberg through bwHPC and the German Research Foundation (DFG) through grant INST 35/1597-1 FUGG. This work was also supported in part by the National Natural Science Foundation of China (Grant No. 62473139), in part by the Hunan Provincial Research and Development Project (Grant No. 2025QK3019), and in part by the Open Research Project of the State Key Laboratory of Industrial Control Technology, China (Grant No. ICT2025B20). This research was partially funded by the Ministry of Education and Science of Bulgaria (support for INSAIT, part of the Bulgarian National Roadmap for Research Infrastructure).

## REFERENCES

- [1] J. Liu, L. Wang, and M.-H. Yang, “Referring expression generation and comprehension via attributes,” in *ICCV*, 2017.
- [2] Z. Yuan, X. Yan, Y. Liao, R. Zhang, S. Wang, Z. Li, and S. Cui, “InstanceRefer: Cooperative holistic understanding for visual grounding on point clouds through instance multi-level contextual referring,” in *ICCV*, 2021.
- [3] R. Liu, C. Liu, Y. Bai, and A. L. Yuille, “CLEVR-Ref+: Diagnosing visual reasoning with referring expressions,” in *CVPR*, 2019.
- [4] H. Qiu, H. Li, Q. Wu, F. Meng, H. Shi, T. Zhao, and K. N. Ngan, “Language-aware fine-grained object representation for referring expression comprehension,” in *MM*, 2020.
- [5] D. Wu, W. Han, T. Wang, X. Dong, X. Zhang, and J. Shen, “Referring multi-object tracking,” in *CVPR*, 2023.
- [6] A. Khoreva, A. Rohrbach, and B. Schiele, “Video object segmentation with language referring expressions,” in *ACCV*, 2019.
- [7] H. Shi, W. Pan, Z. Zhao, M. Zhang, and F. Wu, “Unsupervised domain adaptation for referring semantic segmentation,” in *MM*, 2023.
- [8] R. Li, K. Li, Y.-C. Kuo, M. Shu, X. Qi, X. Shen, and J. Jia, “Referring image segmentation via recurrent refinement networks,” in *CVPR*, 2018.
- [9] H. Shi, H. Li, F. Meng, and Q. Wu, “Key-word-aware network for referring expression image segmentation,” in *ECCV*, 2018.
- [10] S. Seo, J.-Y. Lee, and B. Han, “URVOS: Unified referring video object segmentation network with a large-scale benchmark,” in *ECCV*, 2020.
- [11] C. M. Seibold, S. Reiß, J. Kleesiek, and R. Stiefelhagen, “Reference-guided pseudo-label generation for medical semantic segmentation,” in *AAAI*, 2022.
- [12] R. Dang, J. Feng, H. Zhang, C. Ge, L. Song, L. Gong, C. Liu, Q. Chen, F. Zhu, R. Zhao, and Y. Song, “InstructDET: Diversifying referring object detection with generalized instructions,” in *ICLR*, 2024.
- [13] P. Pramanick, C. Sarkar, S. Paul, R. D. Roychoudhury, and B. Bhowmick, “DoRO: Disambiguation of referred object for embodied agents,” *RA-L*, 2022.
- [14] Y. Fu, R. Wang, Y. Fu, D. P. Paudel, X. Huang, and L. V. Gool, “ObjectRelator: Enabling cross-view object relation understanding in ego-centric and exo-centric videos,” in *ICCV*, 2025.
- [15] J. Saha, C. Chowdhury, I. R. Chowdury, and P. Roy, “Fine grained activity recognition using smart handheld,” in *ICDCN*, 2018.
- [16] G. Laput and C. Harrison, “Sensing fine-grained hand activity with smartwatches,” in *CHI*, 2019.
- [17] C. Lea, R. Vidal, and G. D. Hager, “Learning convolutional action primitives for fine-grained action recognition,” in *ICRA*, 2016.
- [18] Y. Ji, Y. Zhan, Y. Yang, X. Xu, F. Shen, and H. T. Shen, “A context knowledge map guided coarse-to-fine action recognition,” *TIP*, 2020.
- [19] C. Ryali, Y. Hu, D. Bolya, C. Wei, H. Fan, P. Huang, V. Aggarwal, A. Chowdhury, O. Poursaeed, J. Hoffman, J. Malik, Y. Li, and C. Feichtenhofer, “Hiera: A hierarchical vision transformer without the bells-and-whistles,” in *ICML*, 2023.
- [20] L. Wang, B. Huang, Z. Zhao, Z. Tong, Y. He, Y. Wang, Y. Wang, and Y. Qiao, “VideoMAE V2: Scaling video masked autoencoders with dual masking,” in *CVPR*, 2023.
- [21] Y. Li, C.-Y. Wu, H. Fan, K. Mangalam, B. Xiong, J. Malik, and C. Feichtenhofer, “MViT2: Improved multiscale vision transformers for classification and detection,” in *CVPR*, 2022.
- [22] R. Wang, D. Chen, Z. Wu, Y. Chen, X. Dai, M. Liu, L. Yuan, and Y.-G. Jiang, “Masked video distillation: Rethinking masked feature modeling for self-supervised video representation learning,” in *CVPR*, 2023.
- [23] Y. Wang, K. Li, Y. Li, Y. He, B. Huang, Z. Zhao, H. Zhang, J. Xu, Y. Liu, Z. Wang, S. Xing, G. Chen, J. Pan, J. Yu, Y. Wang, L. Wang, and Y. Qiao, “InternVideo: General video foundation models via generative and discriminative learning,” *arXiv preprint arXiv:2212.03191*, 2022.
- [24] K. Peng, A. Roitberg, K. Yang, J. Zhang, and R. Stiefelhagen, “TransDARC: Transformer-based driver activity recognition with latent space feature calibration,” in *IROS*, 2022.
- [25] A. Gritsenko, X. Xiong, J. Djolonga, M. Dehghani, C. Sun, M. Lučić, C. Schmid, and A. Arnab, “End-to-end spatio-temporal action localisation with video transformers,” *arXiv preprint arXiv:2304.12160*, 2023.
- [26] J. Carreira and A. Zisserman, “Quo vadis, action recognition? A new model and the kinetics dataset,” in *CVPR*, 2017.
- [27] R. Goyal, S. E. Kahou, V. Michalski, J. Materzynska, S. Westphal, H. Kim, V. Haenel, I. Fründ, P. Yianilos, M. Mueller-Freitag, F. Hoppe, C. Thurau, I. Bax, and R. Memisevic, “The “something something” video database for learning and evaluating visual common sense,” in *ICCV*, 2017.
- [28] H. Kuehne, H. Jhuang, E. Garrote, T. Poggio, and T. Serre, “HMDB: A large video database for human motion recognition,” in *ICCV*, 2011.
- [29] K. Soomro, A. R. Zamir, and M. Shah, “UCF101: A dataset of 101 human actions classes from videos in the wild,” *arXiv preprint arXiv:1212.0402*, 2012.
- [30] D. Shao, Y. Zhao, B. Dai, and D. Lin, “FineGym: A hierarchical video dataset for fine-grained action understanding,” in *CVPR*, 2020.
- [31] C. Gu, C. Sun, D. A. Ross, C. Vondrick, C. Pantofaru, Y. Li, S. Vijayanarasimhan, G. Toderici, S. Ricco, R. Sukthankar, C. Schmid, and J. Malik, “AVA: A video dataset of spatio-temporally localized atomic visual actions,” in *CVPR*, 2018.
- [32] M. Kim, F. Spinola, P. Benz, and T.-h. Kim, “A\*: Atrous spatial temporal action recognition for real time applications,” in *WACV*, 2024.
- [33] J. Rajasegaran, G. Pavlakos, A. Kanazawa, C. Feichtenhofer, and J. Malik, “On the benefits of 3D pose and tracking for human action recognition,” in *CVPR*, 2023.
- [34] J. Zheng, J. Zhang, K. Yang, K. Peng, and R. Stiefelhagen, “MateRobot: Material recognition in wearable robotics for people with visual impairments,” in *ICRA*, 2024.
- [35] R. Liu, J. Zhang, K. Peng, J. Zheng, K. Cao, Y. Chen, K. Yang, and R. Stiefelhagen, “Open scene understanding: Grounded situation recognition meets segment anything for helping people with visual impairments,” in *ICCVW*, 2023.
- [36] W. Ou, J. Zhang, K. Peng, K. Yang, G. Jaworek, K. Müller, and R. Stiefelhagen, “Indoor navigation assistance for visually impaired people via dynamic SLAM and panoptic segmentation with an RGB-D sensor,” in *ICCHP*, 2022.
- [37] F. Zeng, B. Dong, Y. Zhang, T. Wang, X. Zhang, and Y. Wei, “MOTR: End-to-end multiple-object tracking with transformer,” in *ECCV*, 2022.
- [38] K. Peng, J. Fu, K. Yang, D. Wen, Y. Chen, R. Liu, J. Zheng, J. Zhang, M. S. Sarfraz, R. Stiefelhagen, and A. Roitberg, “Referring atomic video action recognition,” in *ECCV*, 2024.
- [39] J. Li, D. Li, S. Savarese, and S. Hoi, “BLIP-2: Bootstrapping language-image pre-training with frozen image encoders and large language models,” in *ICML*, 2023.
- [40] N. Carion, F. Massa, G. Synnaeve, N. Usunier, A. Kirillov, and S. Zagoruyko, “End-to-end object detection with transformers,” in *ECCV*, 2020.
- [41] L. Zhu, B. Liao, Q. Zhang, X. Wang, W. Liu, and X. Wang, “Vision mamba: Efficient visual representation learning with bidirectional state space model,” in *ICML*, 2024.
- [42] Y. Ma, G. Xu, X. Sun, M. Yan, J. Zhang, and R. Ji, “X-CLIP: End-to-end multi-grained contrastive learning for video-text retrieval,” in *MM*, 2022.
- [43] H. Ding, C. Liu, S. He, K. Ying, X. Jiang, C. C. Loy, and Y.-G. Jiang, “MeViS: A multi-modal dataset for referring motion expression video segmentation,” *TPAMI*, 2025.
- [44] L. Ye, M. Rochan, Z. Liu, X. Zhang, and Y. Wang, “Referring segmentation in images and videos with cross-modal self-attention network,” *TPAMI*, 2022.
- [45] S. Liu, T. Hui, S. Huang, Y. Wei, B. Li, and G. Li, “Cross-modal progressive comprehension for referring segmentation,” *TPAMI*, 2022.
- [46] G. Feng, L. Zhang, J. Sun, Z. Hu, and H. Lu, “Referring segmentation via encoder-fused cross-modal attention network,” *TPAMI*, 2023.

[47] T. Brödermann, C. Sakaridis, Y. Fu, and L. V. Gool, “CAFuser: Condition-aware multimodal fusion for robust semantic perception of driving scenes,” *RA-L*, 2025.

[48] W. Chai, X. Guo, G. Wang, and Y. Lu, “StableVideo: Text-driven consistency-aware diffusion video editing,” in *ICCV*, 2023.

[49] Y. Bu, L. Li, J. Xie, Q. Liu, Y. Cai, Q. Huang, and Q. Li, “Scene-text oriented referring expression comprehension,” *TMM*, 2022.

[50] L. Yu, P. Poirson, S. Yang, A. C. Berg, and T. L. Berg, “Modeling context in referring expressions,” in *ECCV*, 2016.

[51] A. B. Vasudevan, D. Dai, and L. Van Gool, “Object referring in videos with language and human gaze,” in *CVPR*, 2018.

[52] J. Lin, J. Chen, K. Peng, X. He, Z. Li, R. Stiefelhagen, and K. Yang, “EchoTrack: Auditory referring multi-object tracking for autonomous driving,” *T-ITS*, 2024.

[53] T. Deruyttere, S. Vandenhende, D. Grujicic, L. Van Gool, and M.-F. Moens, “Talk2Car: Taking control of your self-driving car,” in *EMNLP*, 2019.

[54] Z. Chen, L. Ma, W. Luo, and K.-Y. K. Wong, “Weakly-supervised spatio-temporally grounding natural sentence in video,” *arXiv preprint arXiv:1906.02549*, 2019.

[55] Y. Su, W. Wang, J. Liu, S. Ma, and X. Yang, “Sequence as a whole: A unified framework for video action localization with long-range text query,” *TIP*, 2023.

[56] K. Gavriluk, A. Ghodrati, Z. Li, and C. G. M. Snoek, “Actor and action video segmentation from a sentence,” in *CVPR*, 2018.

[57] B. McIntosh, K. Duarte, Y. S. Rawat, and M. Shah, “Visual-textual capsule routing for text-based video segmentation,” in *CVPR*, 2020.

[58] A. Radford, J. W. Kim, C. Hallacy, A. Ramesh, G. Goh, S. Agarwal, G. Sastry, A. Askell, P. Mishkin, J. Clark, G. Krueger, and I. Sutskever, “Learning transferable visual models from natural language supervision,” in *ICML*, 2021.

[59] J. Li, D. Li, C. Xiong, and S. Hoi, “BLIP: Bootstrapping language-image pre-training for unified vision-language understanding and generation,” in *ICML*, 2022.

[60] M. Wang, J. Xing, J. Mei, Y. Liu, and Y. Jiang, “ActionCLIP: Adapting language-image pretrained models for video action recognition,” *TNNLS*, 2023.

[61] H. Luo, L. Ji, M. Zhong, Y. Chen, W. Lei, N. Duan, and T. Li, “CLIP4Clip: An empirical study of CLIP for end to end video clip retrieval and captioning,” *Neurocomputing*, 2022.

[62] G. Zhang, J. Ren, J. Gu, and V. Tresp, “Multi-event video-text retrieval,” in *CVPR*, 2023.

[63] W. Wu, H. Luo, B. Fang, J. Wang, and W. Ouyang, “Cap4Video: What can auxiliary captions do for text-video retrieval?” in *CVPR*, 2023.

[64] Y. Chen, J. Wang, L. Lin, Z. Qi, J. Ma, and Y. Shan, “Tagging before alignment: Integrating multi-modal tags for video-text retrieval,” in *AAAI*, 2023.

[65] A. Madasu, E. Aflalo, G. Ben Melech Stan, S.-Y. Tseng, G. Bertasius, and V. Lal, “Improving video retrieval using multilingual knowledge transfer,” in *ECIR*, 2023.

[66] X. Lin, S. Tiwari, S. Huang, M. Li, M. Z. Shou, H. Ji, and S.-F. Chang, “Towards fast adaptation of pretrained contrastive models for multi-channel video-language retrieval,” in *CVPR*, 2023.

[67] Y. Shi, H. Xu, C. Yuan, B. Li, W. Hu, and Z.-J. Zha, “Learning video-text aligned representations for video captioning,” *TOMM*, 2023.

[68] A. Yang, A. Miech, J. Sivic, I. Laptev, and C. Schmid, “Learning to answer visual questions from web videos,” *TPAMI*, 2025.

[69] H. Zhang, A. Sun, W. Jing, L. Zhen, J. T. Zhou, and R. S. M. Goh, “Natural language video localization: A revisit in span-based question answering framework,” *TPAMI*, 2022.

[70] J. Xiao, P. Zhou, A. Yao, Y. Li, R. Hong, S. Yan, and T.-S. Chua, “Contrastive video question answering via video graph transformer,” *TPAMI*, 2023.

[71] Y. Liu, G. Li, and L. Lin, “Cross-modal causal relational reasoning for event-level visual question answering,” *TPAMI*, 2023.

[72] H. Luo, G. Lin, Y. Yao, F. Liu, Z. Liu, and Z. Tang, “Depth and video segmentation based visual attention for embodied question answering,” *TPAMI*, 2023.

[73] A. Yang, A. Miech, J. Sivic, I. Laptev, and C. Schmid, “Just ask: Learning to answer questions from millions of narrated videos,” in *ICCV*, 2021.

[74] S. Castro, N. Deng, P. Huang, M. Burzo, and R. Mihalcea, “In-the-wild video question answering,” in *COLING*, 2022.

[75] D. Gao, L. Zhou, L. Ji, L. Zhu, Y. Yang, and M. Z. Shou, “MIST: Multi-modal iterative spatial-temporal transformer for long-form video question answering,” in *CVPR*, 2023.

[76] L. Li, Z. Gan, K. Lin, C.-C. Lin, Z. Liu, C. Liu, and L. Wang, “LAVENDER: Unifying video-language understanding as masked language modeling,” in *CVPR*, 2023.

[77] J. Chen, D. Zhu, K. Haydarov, X. Li, and M. Elhoseiny, “Video ChatCaptioner: Towards enriched spatiotemporal descriptions,” *arXiv preprint arXiv:2304.04227*, 2023.

[78] H. Zhang, X. Li, and L. Bing, “Video-LLaMA: An instruction-tuned audio-visual language model for video understanding,” in *EMNLP*, 2023.

[79] P. Bagad, M. Tapaswi, and C. G. M. Snoek, “Test of time: Instilling video-language models with a sense of time,” in *CVPR*, 2023.

[80] T. M. Le, V. Le, S. Venkatesh, and T. Tran, “Hierarchical conditional relation networks for video question answering,” in *CVPR*, 2020.

[81] J. Jiang, Z. Chen, H. Lin, X. Zhao, and Y. Gao, “Divide and conquer: Question-guided spatio-temporal contextual attention for video question answering,” in *AAAI*, 2020.

[82] J. Xiao, X. Shang, A. Yao, and T.-S. Chua, “NExT-QA: Next phase of question-answering to explaining temporal actions,” in *CVPR*, 2021.

[83] N. Garcia, M. Otani, C. Chu, and Y. Nakashima, “KnowIT VQA: Answering knowledge-based questions about videos,” in *AAAI*, 2020.

[84] J. Lei, L. Li, L. Zhou, Z. Gan, T. L. Berg, M. Bansal, and J. Liu, “Less is more: ClipBERT for video-and-language learning via sparse sampling,” in *CVPR*, 2021.

[85] W. Guo, Y. Zhang, J. Yang, and X. Yuan, “Re-attention for visual question answering,” *TIP*, 2021.

[86] Y. Li, Y. Fu, T. Qian, Q. Xu, S. Dai, D. P. Paudel, L. V. Gool, and X. Wang, “EgoCross: Benchmarking multimodal large language models for cross-domain egocentric video question answering,” *arXiv preprint arXiv:2508.10729*, 2025.

[87] A. Balaucă, S. Garai, S. Balaucă, R. U. Shetty, N. Agrawal, D. S. Shah, Y. Fu, X. Wang, K. Toutanova, D. P. Paudel, and L. V. Gool, “Understanding the world’s museums through vision-language reasoning,” in *ICCV*, 2025.

[88] J. Li, L. Niu, and L. Zhang, “From representation to reasoning: Towards both evidence and commonsense reasoning for video question-answering,” in *CVPR*, 2022.

[89] M. Gandhi, M. O. Gul, E. Prakash, M. Grunde-McLaughlin, R. Krishna, and M. Agrawala, “Measuring compositional consistency for video question answering,” in *CVPR*, 2022.

[90] G. Li, Y. Wei, Y. Tian, C. Xu, J.-R. Wen, and D. Hu, “Learning to answer questions in dynamic audio-visual scenarios,” in *CVPR*, 2022.

[91] P. Yang, X. Wang, X. Duan, H. Chen, R. Hou, C. Jin, and W. Zhu, “AVQA: A dataset for audio-visual question answering on videos,” in *MM*, 2022.

[92] J. Lei, T. L. Berg, and M. Bansal, “Revealing single frame bias for video-and-language learning,” *arXiv preprint arXiv:2206.03428*, 2022.

[93] K. Li, Y. He, Y. Wang, Y. Li, W. Wang, P. Luo, Y. Wang, L. Wang, and Y. Qiao, “VideoChat: Chat-centric video understanding,” *arXiv preprint arXiv:2305.06355*, 2023.

[94] J. Chung, C.-h. Wu, H.-r. Yang, Y.-W. Tai, and C.-K. Tang, “HAA500: Human-centric atomic action dataset with curated videos,” in *ICCV*, 2021.

[95] C. Feichtenhofer, “X3D: Expanding architectures for efficient video recognition,” in *CVPR*, 2020.

[96] C. Feichtenhofer, H. Fan, J. Malik, and K. He, “SlowFast networks for video recognition,” in *ICCV*, 2019.

[97] R. R. A. Pramono, Y.-T. Chen, and W.-H. Fang, “Spatial-temporal action localization with hierarchical self-attention,” *TMM*, 2021.

[98] S. Wang, R. Yan, P. Huang, G. Dai, Y. Song, and X. Shu, “Com-STAL: Compositional spatio-temporal action localization,” *TCSVT*, 2023.

[99] J. Devlin, M.-W. Chang, K. Lee, and K. Toutanova, “BERT: Pre-training of deep bidirectional transformers for language understanding,” in *ACL*, 2019.

[100] Z. Yu, D. Xu, J. Yu, T. Yu, Z. Zhao, Y. Zhuang, and D. Tao, “ActivityNet-QA: A dataset for understanding complex web videos via question answering,” in *AAAI*, 2019.

[101] P. Sharma, N. Ding, S. Goodman, and R. Soricut, “Conceptual captions: A cleaned, hypernymed, image alt-text dataset for automatic image captioning,” in *ACL*, 2018.

[102] V. Ordonez, G. Kulkarni, and T. Berg, “Im2Text: Describing images using 1 million captioned photographs,” in *NeurIPS*, 2011.

[103] X. Chen, H. Fang, T.-Y. Lin, R. Vedantam, S. Gupta, P. Dollár, and C. L. Zitnick, “Microsoft COCO captions: Data collection and evaluation server,” *arXiv preprint arXiv:1504.00325*, 2015.

[104] A. Kirillov, E. Mintun, N. Ravi, H. Mao, C. Rolland, L. Gustafson, T. Xiao, S. Whitehead, A. C. Berg, W. Lo, P. Dollár, and R. B. Girshick, “Segment anything,” in *ICCV*, 2023.

- [105] L. Jin, G. Luo, Y. Zhou, X. Sun, G. Jiang, A. Shu, and R. Ji, “Ref-CLIP: A universal teacher for weakly supervised referring expression comprehension,” in *CVPR*, 2023.
- [106] A. Dosovitskiy, L. Beyer, A. Kolesnikov, D. Weissenborn, X. Zhai, T. Unterthiner, M. Dehghani, M. Minderer, G. Heigold, S. Gelly, J. Uszkoreit, and N. Houlsby, “An image is worth 16x16 words: Transformers for image recognition at scale,” in *ICLR*, 2021.
- [107] S. Zhang, S. Roller, N. Goyal, M. Artetxe, M. Chen, S. Chen, C. Dewan, M. T. Diab, X. Li, X. V. Lin, T. Mihaylov, M. Ott, S. Shleifer, K. Shuster, D. Simig, P. S. Koura, A. Sridhar, T. Wang, and L. Zettlemoyer, “OPT: Open pre-trained transformer language models,” *arXiv preprint arXiv:2205.01068*, 2022.
- [108] D. P. Kingma and J. Ba, “Adam: A method for stochastic optimization,” in *ICLR*, 2015.
- [109] A. Nagrani, S. Yang, A. Arnab, A. Jansen, C. Schmid, and C. Sun, “Attention bottlenecks for multimodal fusion,” in *NeuIPS*, 2021.
- [110] D. Zong and S. Sun, “McOmet: Multimodal fusion transformer for physical audiovisual commonsense reasoning,” in *AAAI*, 2023.
- [111] T.-Y. Lin, P. Goyal, R. Girshick, K. He, and P. Dollár, “Focal loss for dense object detection,” in *ICCV*, 2017.
- [112] OpenAI, “ChatGPT: Optimizing language models for dialogue,” <https://openai.com/>, 2022.